

NATIONAL AERONAUTICS AND SPACE ADMINISTRATION

Technical Report No. 32-844

The JPL High-Impact Program—1965

J. L. Adams

FACILITY FORM 602

N 66 - 16 154	
(ACCESSION NUMBER)	(THRU)
33	1
(PAGES)	(CODE)
CR 69919	32
(NASA CR OR TMX OR AD NUMBER)	(CATEGORY)

GPO PRICE \$ _____

CFSTI PRICE(S) \$ _____

Hard copy (HC) 2.00

Microfiche (MF) .50

ff 653 July 65

JET PROPULSION LABORATORY
CALIFORNIA INSTITUTE OF TECHNOLOGY
PASADENA, CALIFORNIA

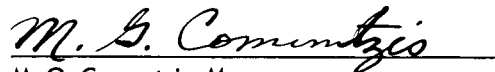
February 1, 1966

NATIONAL AERONAUTICS AND SPACE ADMINISTRATION

Technical Report No. 32-844

The JPL High-Impact Program—1965

J. L. Adams



M. G. Comuntzis, Manager
Lunar Spacecraft Development Section

JET PROPULSION LABORATORY
CALIFORNIA INSTITUTE OF TECHNOLOGY
PASADENA, CALIFORNIA

February 1, 1966

Copyright © 1966
Jet Propulsion Laboratory
California Institute of Technology
Prepared Under Contract No. NAS 7-100
National Aeronautics & Space Administration

CONTENTS

I. Introduction	1
II. Test Facilities	4
III. Packaging	8
IV. Gas Chromatograph	10
V. S-Band Transmitter	13
VI. Batteries	15
VII. Mechanisms	18
VIII. Miscellaneous Electronic-Component Testing	21
A. Capacitors	21
B. Diodes	21
C. Microcircuits	21
D. Resistors	21
E. Transistors	22
References	24

TABLES

1. High-impact battery tests	15
2. Impact tests of ball bearings and bushings	18

FIGURES

1. Spring-mass system	2
2. Response spectrum for vibration amplification	2
3. Response spectra for various shock shapes	3
4. Spectra for rectangular, triangular, and sawtooth shocks	3
5. Compressed-air gun, 6-in. diameter	5

FIGURES (Cont'd)

6. Schematic of compressed-air gun, 6-in. diameter	5
7. Impacted balsa blocks	6
8. Prototype air turbine mounted in a 6-in. projectile	6
9. Compressed-air gun, 3-in. diameter	6
10. Compressed-air gun, 22-in. diameter	7
11. Compressed-air gun, 22-in. diameter, with piston	8
12. Test module for conformal coatings	9
13. High-impact cordwood chassis	9
14. Schematic of gas chromatograph	10
15. High-impact gas chromatograph	11
16. Interior of gas chromatograph	11
17. Gas-chromatograph sample valve	11
18. Gas-chromatograph ionization detector	12
19. Gas-chromatograph pressure regulator	12
20. S-band transmitter schematic	13
21. DC side of Module No. 1—S-band transmitter	13
22. RF side of Module No. 1—S-band transmitter	14
23. Module No. 2 (foreground)—S-band transmitter	14
24. High-impact crystal	14
25. Ruggedized S-band turnstile antenna	14
26. Battery impact acceleration directions	15
27. Six-cell battery before impact	17
28. Six-cell battery plates after impact	17
29. Alternate gas-chromatograph sample valve	18
30. Bearing spring mount	19
31. Exploded view of ruggedized motor	19
32. High-impact-resistant turbine	20
33. Pressure vessel and fixtures after test	20
34. Integrated circuit after test	22
35. Hi-Meg resistors after test	22
36. Transistor failure	23

ABSTRACT

16154

This Report summarizes the progress of the JPL High-Impact Survival Program since September, 1964. During this period, impact work has increased in intensity at JPL because of such efforts as the *Voyager* Landing Capsule and the *Surveyor* Critical Data Recorder. Specific efforts underway include the investigation of mechanism elements and electronic packaging techniques under impact and the development of a ruggedized gas chromatograph, an impact-resistant 3-w solid-state S-band transmitter, impact-resistant flat-plate batteries, and ruggedized antennas. The JPL development goal has remained the survival of a 10,000-g impact. Preimpact velocities up to 500 ft/sec are under consideration in order to cover possible Mars hard-landing situations. Test facilities have been developed in order to provide the necessary velocities. This Report presents the status of these various efforts along with experimental results where pertinent. It should be noted that this Report is concerned only with impacts in which the impact velocity is well below wave propagation velocities. The phenomena associated with hypervelocity impacts are of a much different nature and are of concern to the spacecraft engineer chiefly in conjunction with meteoroid damage.

Author

I. INTRODUCTION

In order to intelligently design lunar and planetary landers, it is necessary to have some feeling for the effects of high impact upon electromechanical equipment. The trade-off between retardation system, energy absorber, and payload impact environment is a critical one in any lander design. The ability to build impact-resistant equipment results in greater flexibility in this trade-off and, therefore, in the total system design. The techniques of building impact-resistant equipment can be used to develop rough landers, build "hardened" diagnostic packages for soft landers, and provide increased survival margins in the event of nonstandard descents and land-

ings. They can also be used to make spacecraft equipment less susceptible to ordinary handling and launch damage.

Vibration is the dominant mechanical environment for flyby and orbiting spacecraft. Most engineers involved with the development of spacecraft hardware have developed a good feeling for the response of physical systems to vibration. However, they sometimes tend to overestimate the severity of impact loading. This overestimation is probably due to lack of experience with impact loading, the dramatic nature of high-impact tests, and the tendency to equate a 1000-g shock with a 1000-g shake. For those

unfamiliar with shock loading, it might be worthwhile at this time to examine the effects of transient inputs upon a single-degree-of-freedom, undamped, linear spring-mass system.

Although extremely simple, the spring-mass system has many advantages as an example of elastic behavior. First of all, if the spring is considered to be massless, wave propagation effects may be ignored. Secondly, the dynamic response of a spring-mass system is easily visualized by most engineers, which allows rapid comparison of the effects of various inputs. Thirdly, although it is a single-degree-of-freedom system, the solution to the spring-mass problem is quite typical. It proceeds in the same manner as that of classical multi-degree-of-freedom systems, which are decoupled by use of generalized coordinates so that individual modes can be handled separately.

The spring-mass system can be diagrammed as shown in Fig. 1: The quantities x and x_g represent displacements of the mass and ground, respectively, away from their initial equilibrium positions. Spring distortion, x_d , is

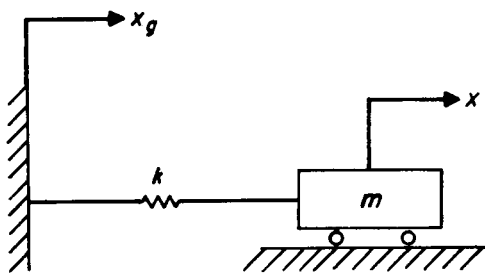


Fig. 1. Spring-mass system

equal to $x - x_g$. This system is representative of a vibration test if the ground is considered to be the shake table and the mass and spring are considered to be an elastic test specimen. It is representative of an impact test if the ground is considered to be the carriage of the shock machine and the mass and spring are considered to be an elastic test specimen. In a typical test, the dynamic excitation can be measured by attaching an accelerometer to the table or carriage (the ground). The quantity of interest, in many instances, is the strain in the elastic test specimen (x_d , the spring distortion).

A simple means of examining this spring distortion as a function of various ground acceleration inputs is by means of response spectra. Response spectra are plots of the peak response of a linear, variable-frequency, single-degree-of-freedom oscillator to a specific input, as a func-

tion of the oscillator frequency. Good discussions of response spectra can be found in Refs. 1 and 2. Typically, response spectra compare a normalized displacement with a normalized input time. A familiar one is the response spectrum for vibration amplification in a spring-mass system shown in Fig. 2. This curve shows normalized

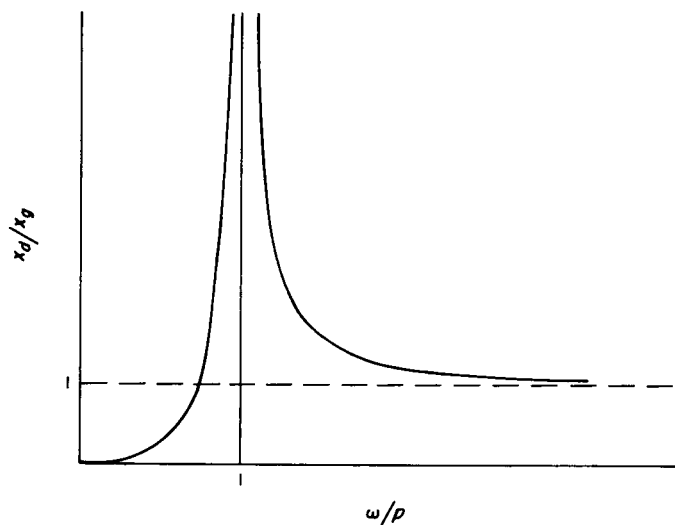


Fig. 2. Response spectrum for vibration amplification

maximum spring distortion for a ground displacement excitation as a function of frequency ratio. In an actual physical situation the normalized distortion never becomes infinite because of damping, spring nonlinearity, and failures. However, amplifications of 20 to 50 are not uncommon in ordinary spacecraft equipment.

For discussing nonrepetitive shock excitations, it is more convenient to talk about the ratio of periods rather than the ratios of frequencies. Normalized distortions can be plotted against the ratio τ/T , where τ is a characteristic shock time dimension and T is $2\pi/p$, or the period of natural vibration of the spring-mass system.

Figure 3 shows spectra resulting from shocks of four different shapes and identical impulse. The ordinate represents $\frac{x_d(\max)}{Am/k}$ or $\frac{x_d(\max)}{A/p^2}$. This is merely the maximum spring distortion normalized with the spring distortion which would result from a steady ground acceleration of magnitude A . The quantity $x_d(\max)$ is the maximum distortion attained either during or after the excitation, and $p = \sqrt{k/m}$, where p is the natural frequency of the oscillator, k is the spring constant, and m is the mass. Note that for small values of τ/T , the shape of the pulse is unimportant. At large values of τ/T , the shape of the

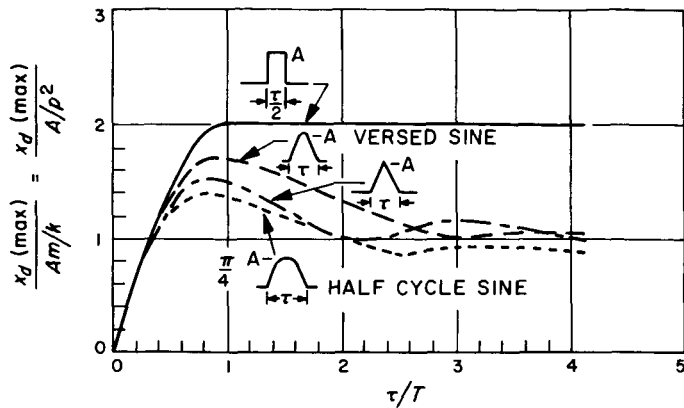


Fig. 3. Response spectra for various shock shapes

pulse (especially the rising portion) can result in an amplitude gain factor of 2.

Figure 4 compares spectra resulting from a rectangular pulse, a leading peak sawtooth, a trailing peak sawtooth, and a symmetrical triangular pulse, all with equal impulse and peak amplitude.

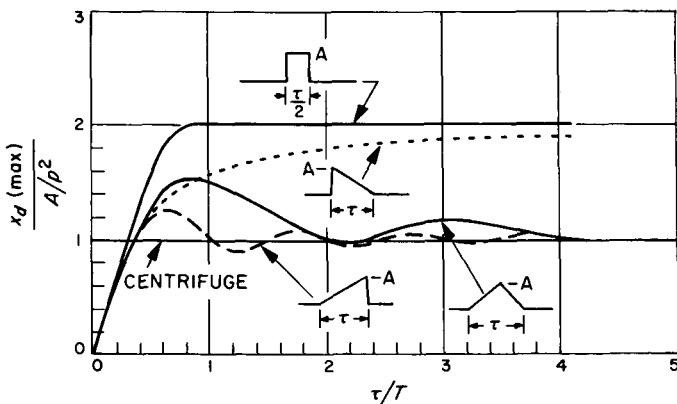


Fig. 4. Spectra for rectangular, triangular, and sawtooth shocks

There are several interesting points which can be seen from these shock spectra:

1. The maximum amplification is 2, as opposed to an infinite theoretical amplification at resonance in an undamped sinusoidally excited spring-mass system. The exact amplification in a shock is a function of the nature of the pulse and the pulse length. The rate of onset of acceleration of a shock is called the *jerk* (third time derivative of displacement). When the jerk is infinite (sharp shock), the normalized spring distortion in the ideal spring-mass system approaches 2 providing that

the pulse length is sufficiently long. In the case of a rectangular pulse, the normalized distortion is 2 providing that the length of the pulse is equal to or greater than half of the period of natural vibration of the spring-mass system. When the jerk is low (approaching a centrifuge value), the normalized spring distortion approaches unity.

2. In order to "attenuate" shock response, it is necessary to ensure that τ/T is very small. This is difficult to achieve in practice if the impacts are severe. For instance, to ensure that the normalized response of an ideal spring-mass system to a rectangular pulse be below unity (no gain), τ/T must be less than 0.15. If the pulse were one msec long, this would require that T be at least 6.6 msec. This corresponds to a spring-mass natural frequency of 150 cps, which is very low for impact-resistant equipment. Such a spring-mass system would suffer a peak spring distortion of over 4 in. if exposed to a 10,000-g rectangular ground shock lasting 1 msec. This is an unrealistic excursion for practical equipment design.

3. Exact shock shape is relatively unimportant in engineering work. In discussing normalized shock pulses (peak amplitude equal to unity), Fung and Barton (Ref. 2) state:

"In specifying a pulse form for engineering design purposes, there is little point in specifying the exact manner the pulse varies with time; in particular, the time history after the peak value of the pulse is reached is unimportant. Only the total impulse, the rise time, and when greater accuracy is desired, the time history of the rising curve, need be specified."

Obviously, when actual equipment is concerned, responses cannot be as cleanly represented as they can for the linear, single-degree-of-freedom case. However, the basic considerations still hold. Amplifications are much lower under transient loads than under vibration, and structural stresses are accordingly less. Exact shock pulse shapes are not extremely critical for design purposes, so long as the peak level, the onset rate, and some measure of energy content are specified. A general description of shape and a representative length are adequate for specifying energy content. Energy content can also be specified by a description of the general shape and the total velocity change during the impact. An excellent discussion of shock testing and shock shape specification can be found in Ref. 3.

An involved theoretical treatment of shock response is not in order at this time. Equipment designed to survive 10,000-g shocks must obviously be more rugged than ordinary spacecraft equipment. However, such equip-

ment is far from unfeasible. A typical *Ranger-Mariner* electronic module is a flanged $6 \times 6 \times 0.090$ -in. magnesium plate with circuit boards bonded to each side. A corresponding high-impact module might consist of a flanged $2 \times 4 \times \frac{1}{4}$ -in. or $3 \times 6 \times \frac{3}{8}$ -in. plate. The remainder of this Report will discuss specific high-impact testing and development performed at JPL. The examples

of hardware presented will further clarify the physical nature of equipment designed for high-impact survival.

JPL has maintained a program of high-impact technology since 1959. Reference 4 summarizes the program up through September 1964. This Report summarizes more recent developments.

II. TEST FACILITIES

The goal of the JPL high-impact program has been to develop the technology necessary for building spacecraft equipment capable of withstanding impacts of up to 10,000 *g*'s peak amplitude from preimpact velocities of several hundred ft/sec. The majority of the testing has been done either on a drop tower (capable of accelerating a test specimen to 50 ft/sec) or on the JPL horizontal impact machine (a bungee-powered slingshot capable of accelerating a test specimen to 200 ft/sec). Details of these facilities are contained in Ref. 4. A rectangular acceleration-vs-time curve with a 10,000-*g* peak resulting from a 200-ft/sec impact velocity has a duration of approximately $\frac{3}{8}$ msec. According to the previous discussion of shock spectra, this pulse length would result in maximum amplification in a spring-mass system providing that the natural frequency was above 750 cps.

Before this Report period, velocities were limited to 200 ft/sec (the approximate impact velocity of the *Ranger* hard-lander capsules). In order to extend the test program to be more compatible with possible Mars hard-landers and equipment with lower resonant frequencies (batteries and larger structural elements), JPL has recently been investigating impact phenomena from velocities of up to 500 ft/sec. In order to accelerate test specimens to this higher energy level, three compressed-air guns have been developed by the Engineering Mechanics Division. These guns have bores of 3, 6, and 22 in. They are similar in principle and in operation and differ only in payload capability. The guns are used to accelerate test specimens to the desired impact velocities. The impacts are obtained by decelerating the projectiles with the use of a deformable material, such as wood. Instrumentation is identical to that used with the sling-shot

and the drop tower. Preimpact velocity is measured using either break-wires or a light-trap. Accelerometer traces are obtained by means of a trailing cable.

Figure 5 is a picture of the 6-in. gun. It is capable of accelerating a mass of 25 lb to 500 ft/sec. Figure 6 is a schematic of the gun. It consists of a 2-ft-diam \times 9-ft-long storage chamber, two 6-in.-diam barrels 18 ft. long, and various pipe fittings. Two barrels are used to minimize recoil. The projectiles are loaded into the barrels and held under slight tension against O-ring seals. Tension is provided by rods which are fitted with turnbuckles and connect the two projectiles by means of a clevis, a yoke, and a shear pin. The storage chamber is then pressurized until the shear pin fails. Various velocities can be obtained by controlling the shear area. A high-pressure, unrestricted air bottle is used to control the time of triggering within a smaller time increment than could be obtained with the main pressurization system. Figure 7 shows two $8\frac{1}{2}$ -in.-square \times 35-in.-long blocks of balsa which were impacted with 25-lb projectiles traveling at 500 ft/sec so that the effect of velocity on energy absorption could be determined. Figure 8 shows a ruggedized air turbine in a test fixture mounted to the nose plate of a typical projectile. The accelerometer cable unwinds from the cylinder on the trailing end.

Figure 9 shows the 3-in.-diam gun. This gun is similar to the 6-in.-diam gun in operation except that on the 3-in.-diam gun a manually broken tension link is used for triggering rather than a shear pin. As in the 6-in.-diam gun, a flange between the barrel and the pressure chamber contains an O-ring which acts as a seal with the

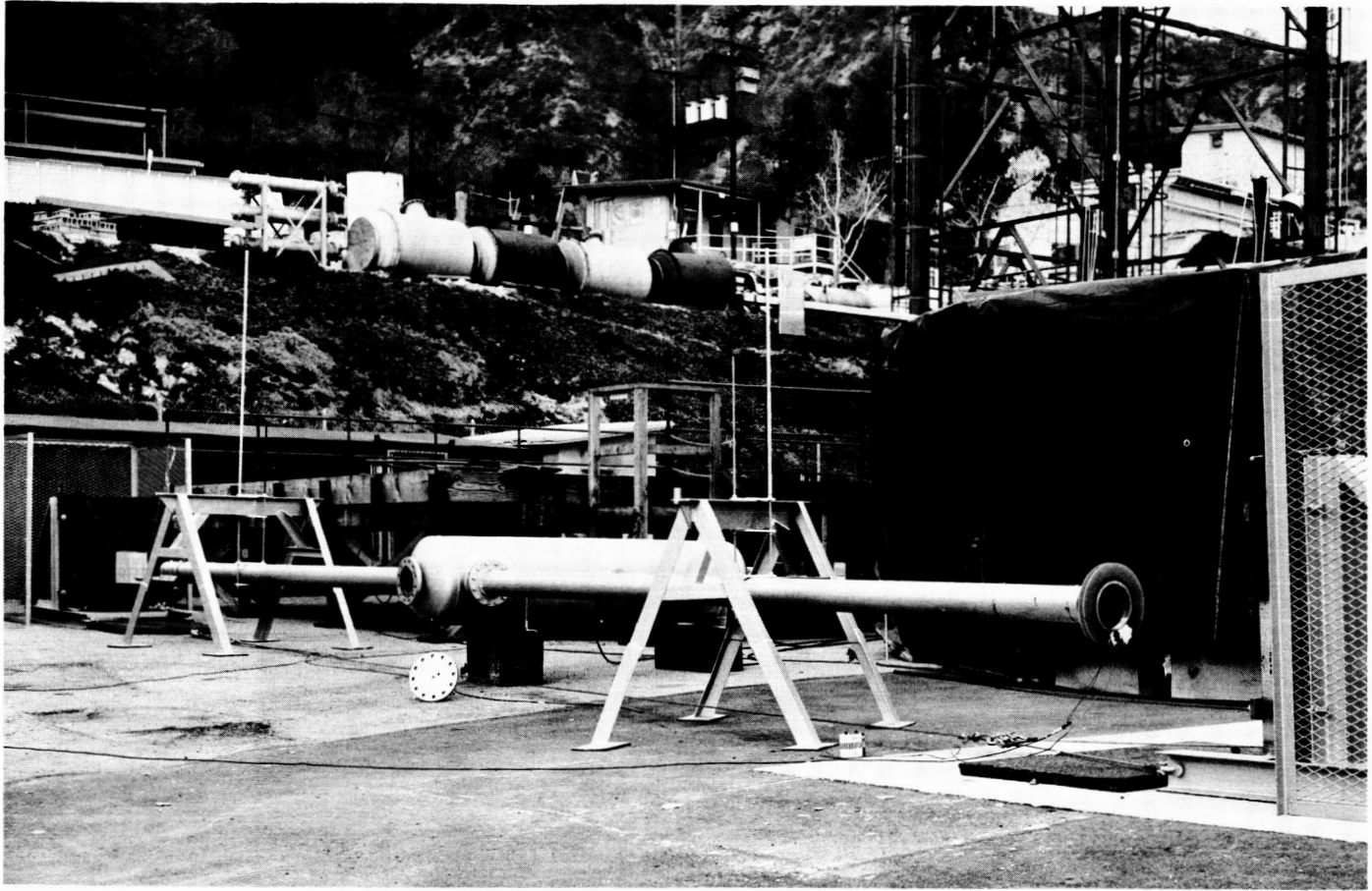


Fig. 5. Compressed-air gun, 6-in. diameter

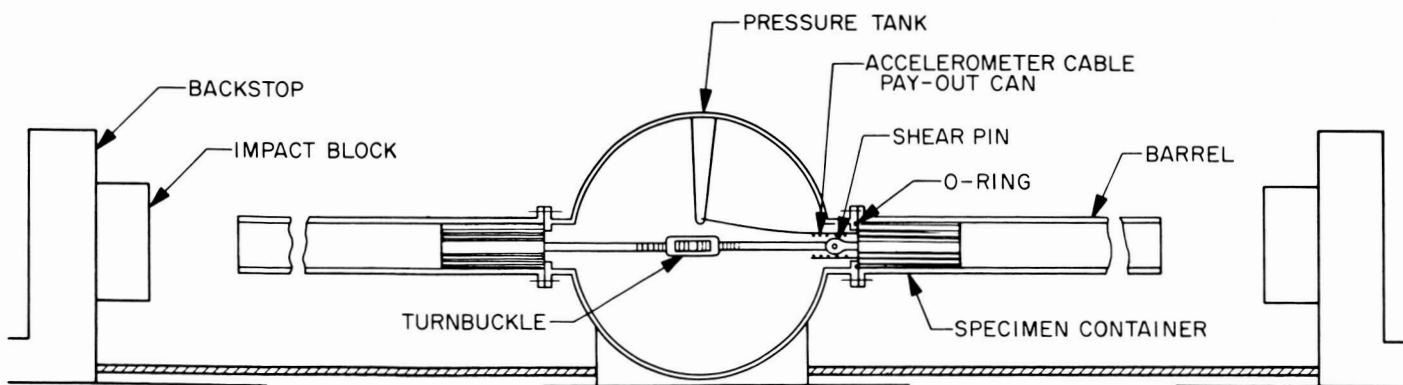


Fig. 6. Schematic of compressed-air gun, 6-in. diameter

projectile before firing. A rod extends from the back of the projectile through a gland in the end of the pressure chamber. This rod is necked down at the projectile end and threaded at the other end. The O-ring is seated by tightening a nut which is threaded onto the end of the

rod which projects through the pressure tank. In order to fire the gun, the chamber is pressurized and the nut is tightened until the rod fails at the necked section. This gun is capable of accelerating approximately 1 lb to 500 ft/sec.

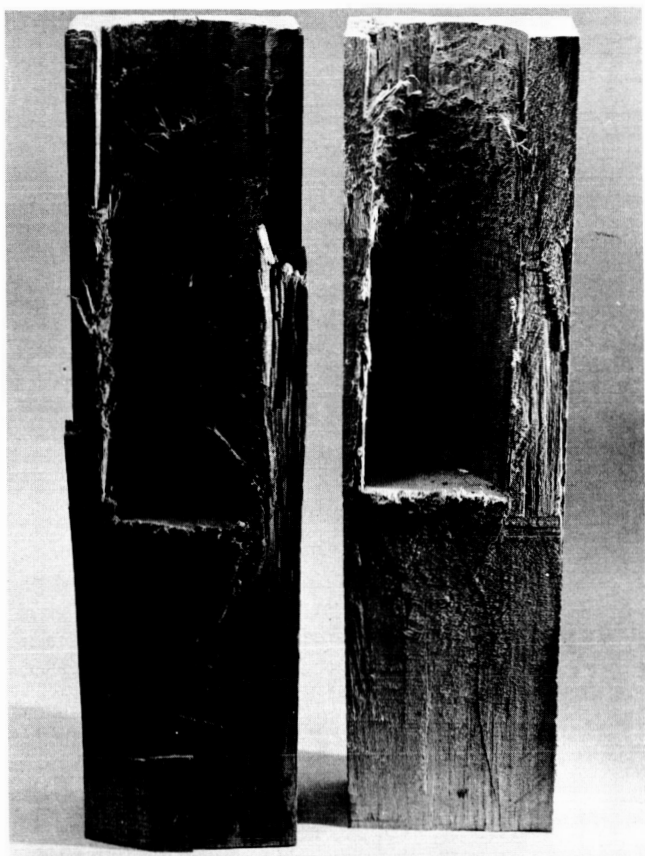


Fig. 7. Impacted balsa blocks

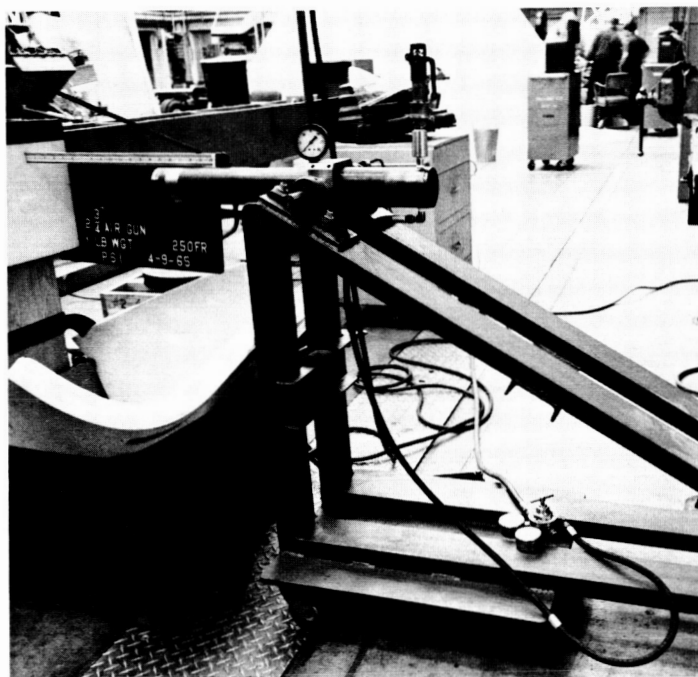


Fig. 9. Compressed-air gun, 3-in. diameter

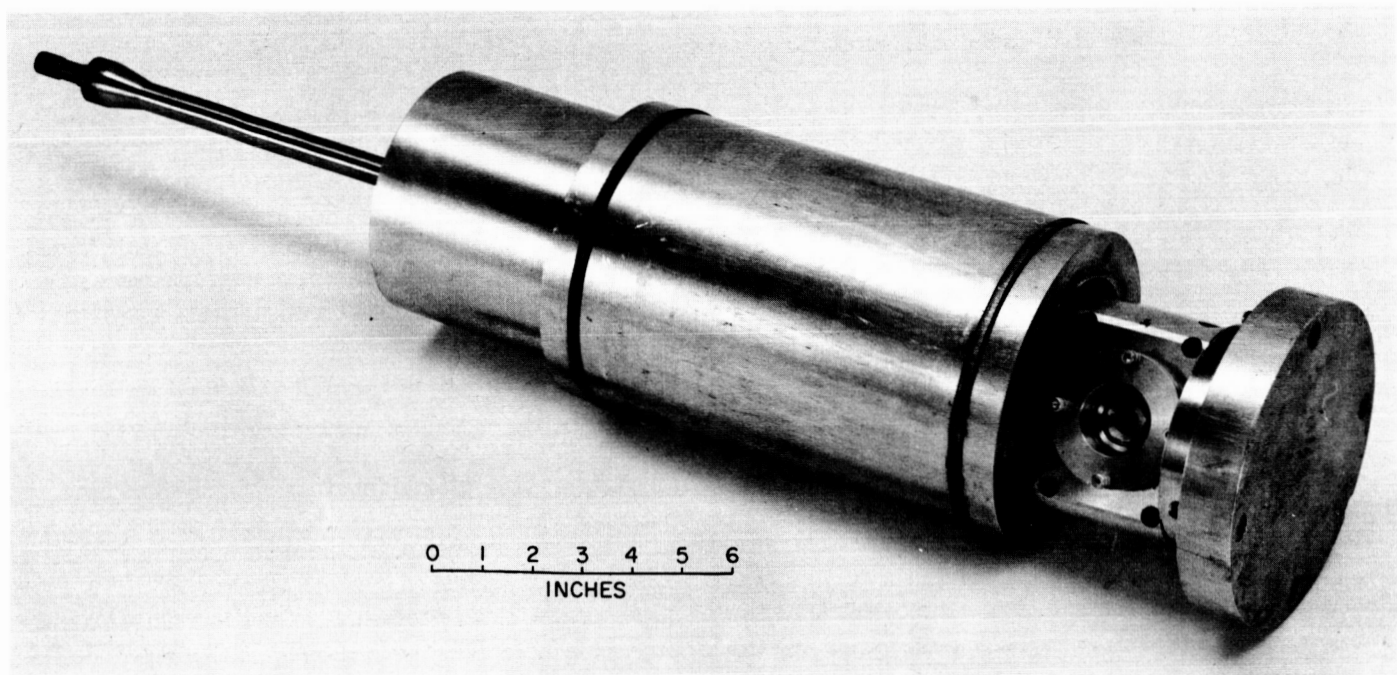


Fig. 8. Prototype air turbine mounted in a 6-in. projectile

Figure 10 shows the 22-in.-diam gun. The pressure section is 12 ft long. With the 18-ft-long barrel shown in Fig. 10, the gun is capable of accelerating approximately 400 lb to 500 ft/sec. It is similar in operation to the 6-in.-diam and the 3-in.-diam guns in that it uses an O-ring and a flange for sealing before being fired. Triggering is either by means of a shear-pin clevis linkage, or by means of weakening a tension link with a pin fired from a Ramset. The 22-in.-diam gun can be used either to accelerate a projectile containing the test specimen or in conjunction with a piston and push rod to accelerate

the test specimen. The projectile mode of operation sacrifices less of the total payload capability to test fixture. However, the dimensions of the test specimen are necessarily limited. If a piston is used to accelerate the test article, the pusher assembly must be designed to survive the acceleration and a rather abrupt deceleration, since it must be stopped short of the impact surface. Figure 11 shows the gun equipped with a pusher assembly developed for impact-testing air-bag decelerators. This assembly is used in conjunction with a short (6-ft) barrel. The pusher and the specimen are accelerated to veloci-

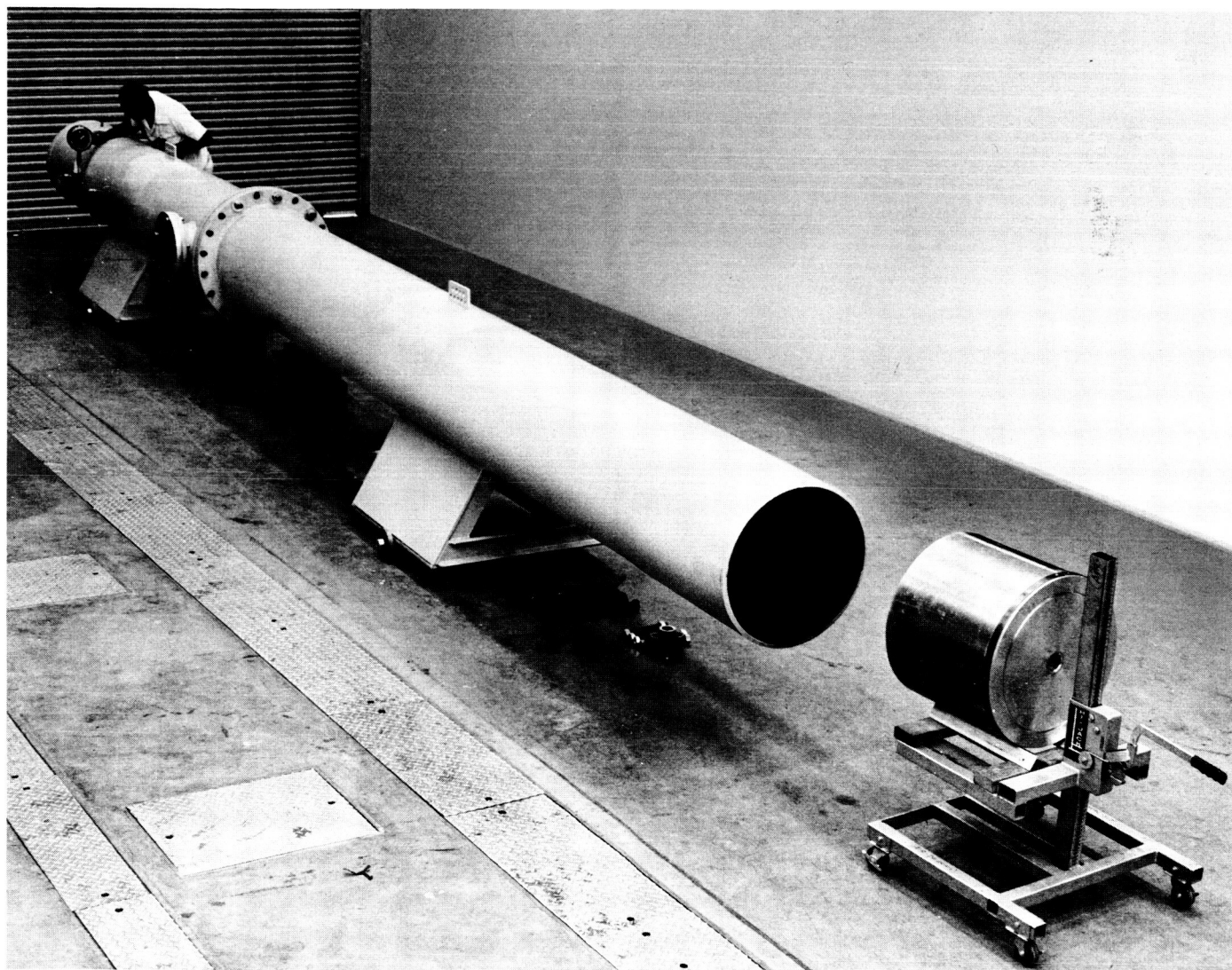


Fig. 10. Compressed-air gun, 22-in. diameter

ties up to 200 ft/sec and then stopped by use of a crushable sleeve around the pusher. The decelerator and

its simulated payload are then allowed to fly free to the target.

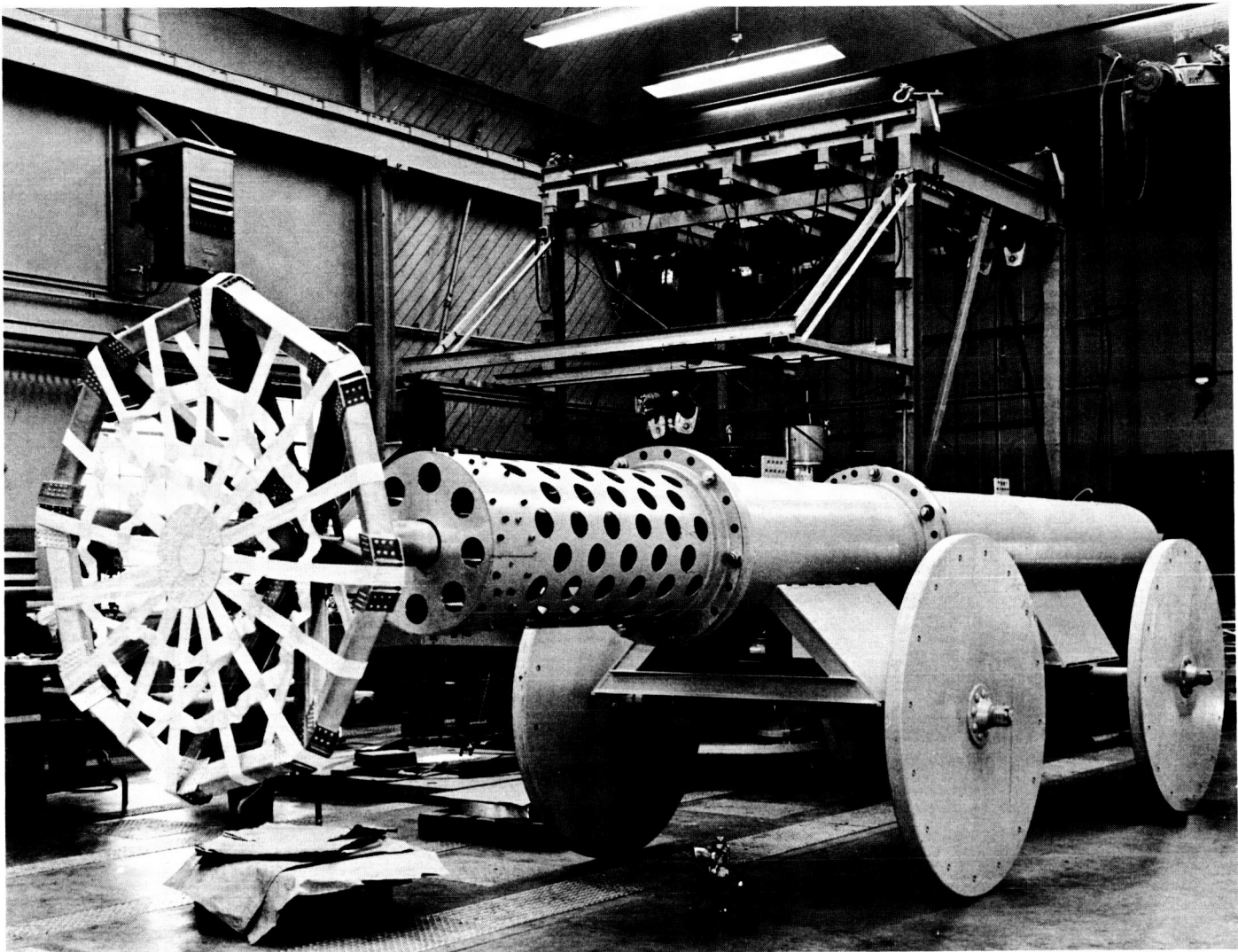


Fig. 11. Compressed-air gun, 22-in. diameter, with piston

III. PACKAGING

An investigation of high-impact packaging is underway in the Engineering Mechanics Division of JPL. Most high-impact equipment built to date has utilized terminal boards or printed circuit boards bonded to extremely

rigid chassis. Potting has been minimized in order to minimize losses in high-frequency equipment, in order to simplify inspection and rework, and because 100% potting is not necessary at 10,000 g's. Components have been,

instead, supported by being hard-mounted either to the terminal or printed circuit boards or directly to structure (see Ref. 4).

The present effort is for the purpose of investigating alternate approaches which allow greater packaging efficiency and are more compatible with microcircuitry and 3-D interconnection techniques. Embedding, coating, and bonding materials are also being investigated under the impact environment. As an example, Fig. 12 shows a mocked-up module containing components supported by a coating of polyurethane (Solithane 113-300). This module

to the carriage of the horizontal impact machine with 3M Scotchweld EC-1614 and impacted at levels in excess of 10,000 g's from 200 ft/sec with no visible damage either to the potting material or the adhesive. A functional *Mariner Mars* A/PW welded module was potted into a cavity in a rigid test fixture with a Solithane formulation and impacted in all significant directions at increasing acceleration levels. The electrical performance of the module was not degraded by tests up to and including 7500 g's peak amplitude from 170 ft/sec. A test at 10,000 g's peak amplitude from 185 ft/sec failed the module. Subsequent examination showed the failure to be in a 2N861 transistor, which is not an impact-resistant component. The packaging techniques appeared fully adequate for the 10,000-g environment.

A *Mariner Mars* Attitude Control Gyro Switch welded module and a Rocket Radar module containing integrated circuits assembled in cordwood fashion were also tested. The Gyro Switch survived impacts in excess of 10,000 g's from 200 ft/sec with no electrical or mechanical degradation. The Rocket Radar module was inoperative after a test of 8,000 g's peak amplitude from 200 ft/sec. Once again, the failure was due to a component failure. The packaging technique was not at fault.

Figure 13 shows a prototype high-impact cordwood chassis. The modules are supported in an egg-crate box beam. The package is shown in the testing fixture. Such units have survived impacts of up to 10,000 g's peak amplitude from 200 ft/sec in all principal directions with no damage to chassis or potting.

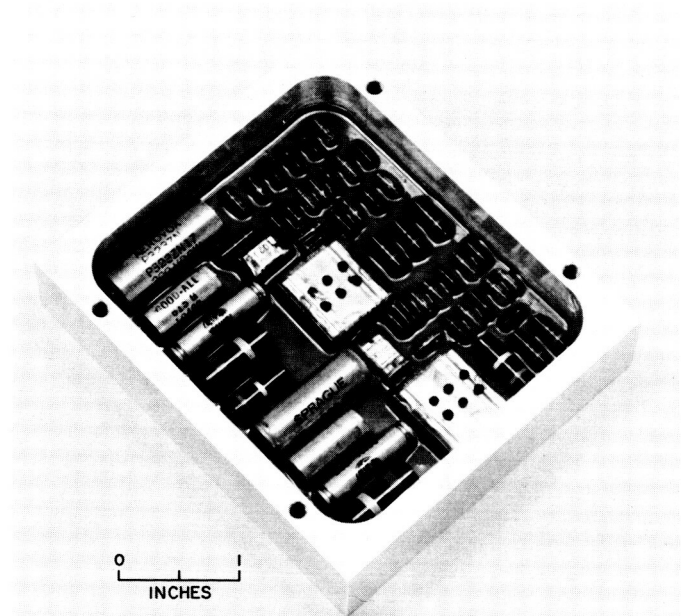


Fig. 12. Test module for conformal coatings

was impacted at increasing acceleration levels in order to measure the load-carrying capacity of Solithane coating. The two large rectangular glass-cased capacitors were broken loose at impacts of approximately 5,000 g's average amplitude from 130 ft/sec. One large cylindrical capacitor was lost at an impact of 7,500 g's average amplitude from 150 ft/sec. However, all other components were supported by the polyurethane up through impacts of 10,000 g's average amplitude from 200 ft/sec.

Dummy welded-cordwood modules embedded with Emerson and Cuming Stycast 1090/11 have been bonded

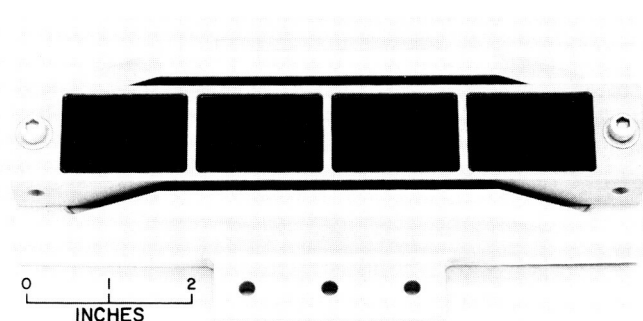


Fig. 13. High-impact cordwood chassis

IV. GAS CHROMATOGRAPH

A ruggedized gas chromatograph is under development as a joint effort between the Engineering Mechanics Division and the Space Sciences Division. The basis for the instrument was the Mars-atmospheric scientific-feasibility gas-chromatograph breadboard which was developed under a previous Advanced Development task. The instrument does not contain the programmer required for fully automatic operation, or an integrator such as would be found in a flight instrument. However, components of the type used in these circuits are present in the signal processing unit of the ruggedized instrument. Figure 14 is a schematic of the instrument. This particular version of the gas chromatograph is capable of detecting argon, nitrogen, and carbon dioxide. However, the capability of the instrument could be increased merely by adding more stages of columns, detectors, and associated electronics.

Figures 15 and 16 are photographs of the prototype instrument. The instrument has not yet been impacted as a unit. However, all questionable components have been tested and redesigned and ruggedized when necessary. The chassis itself has been conservatively designed so that no problems are expected due to dynamic deflections. The electrical-components testing section of this report includes specific electrical-component tests which were performed in conjunction with the gas chromatograph. The majority of the component testing has been performed on the horizontal test machine. However, resonant frequencies in the chromatograph are sufficiently high so that most test results should be valid for a 10,000-g level from a 500 ft/sec velocity.

The electronic components have been packaged in conventional manner between terminals on printed circuit

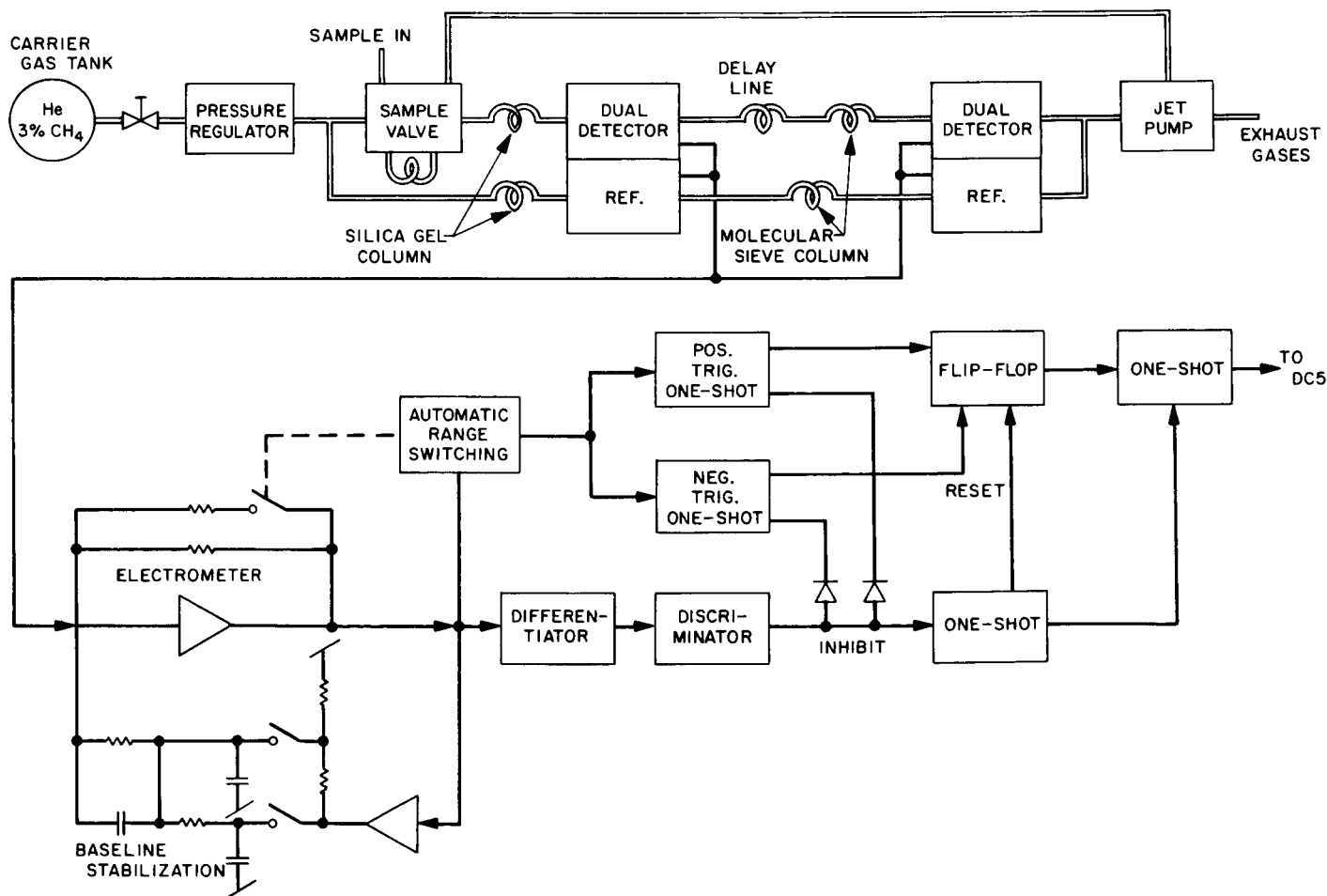


Fig. 14. Schematic of gas chromatograph

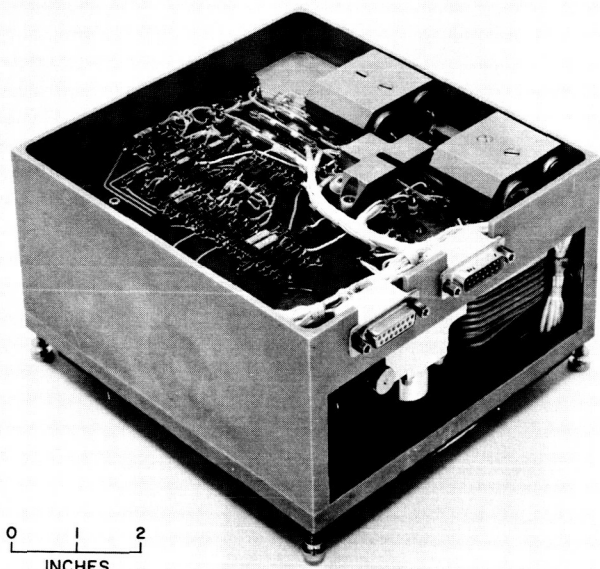


Fig. 15. High-impact gas chromatograph

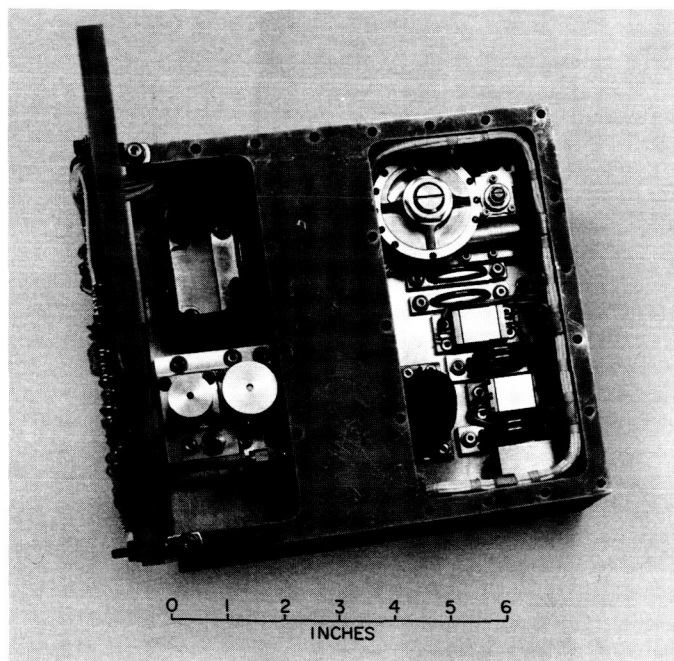


Fig. 16. Interior of gas chromatograph

boards. The heavier components have been spot-bonded in place. The boards and components have been coated with Solithane 113-300. A few large components (mylar capacitors) have been clamped to the chassis. All wiring has been securely clamped and bonded in place.

Structurally, the unit consists of two plates (the electronic mounting surfaces) separated by a stiff central member (the pressure bottle for the carrier gas) and the side and end walls of the unit. The unit was designed to survive a 10,000-g shock when mounted as a simply supported beam. With the exception of the supply line from the carrier gas bottle, all plumbing is integral with the chassis. All valves, regulators, columns, and detectors, as well as the sample loop, the delay line, and the jet pump, are mounted rigidly to the chassis with O-ring seals.

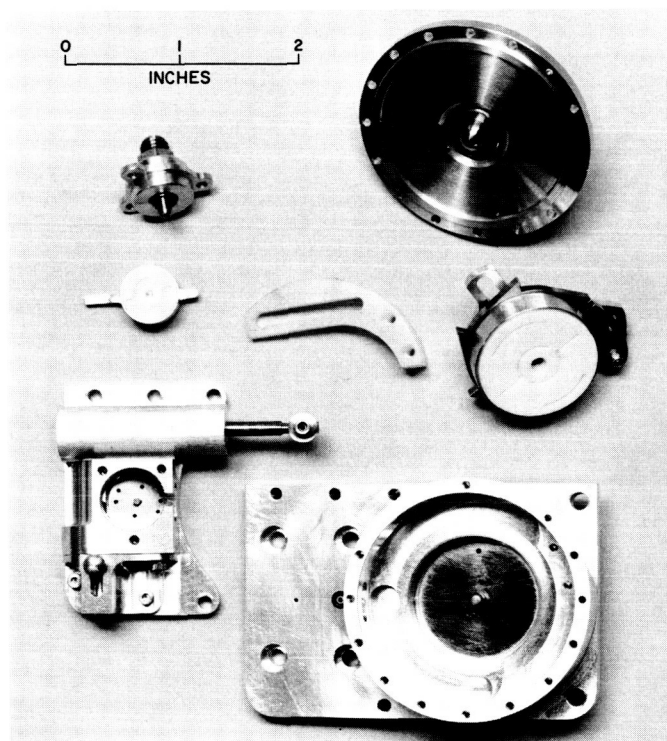


Fig. 17. Gas-chromatograph sample valve

Figures 17-19 show exploded views of the sample valve, an ionization detector, and the pressure regulator. These devices were all developed specifically to survive the high-impact environment. The sample valve is a three-position rotary gas valve used to interconnect the sample source, the carrier gas, the vacuum line from the jet pump, the sample loop, and the analysis line in various combinations. The valve is powered by regulated carrier gas which is in turn controlled by a solenoid. The device weighs 8 oz. The ionization detector incorporates adjustable electrodes and a maximum of support to all critical elements. The pressure regulator regulates the 3,000-lb carrier gas supply to 70 psi. It is a two-stage device with an adjustment in the low pressure stage and weighs 5 oz.

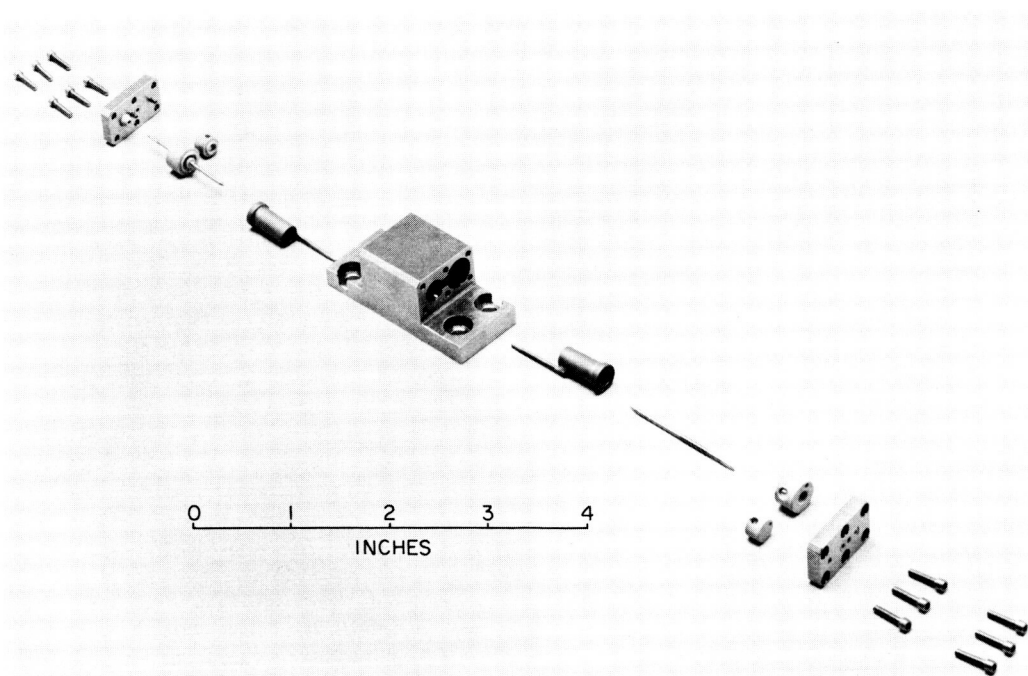


Fig. 18. Gas-chromatograph ionization detector

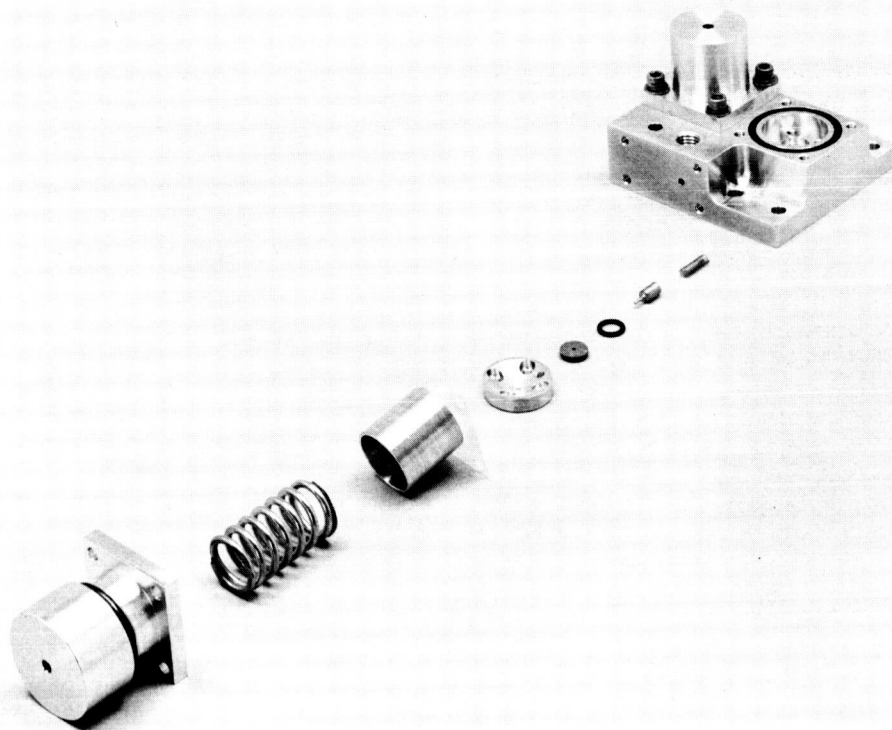


Fig. 19. Gas-chromatograph pressure regulator

The gas chromatograph is presently undergoing performance and impact testing and continued development. It is not now known what the final performance, weight, or impact-survival capability of the instrument

will be. However, it is felt that the original goal of proving the feasibility of ruggedizing a complex, sensitive, and electromechanically typical scientific instrument has been attained.

V. S-BAND TRANSMITTER

The development of a ruggedized, 3-w, solid-state, S-band transmitter is being carried on as a joint effort between the Telecommunications Division and the Engineering Mechanics Division. Figure 20 is a schematic of the transmitter, which is packaged in three modules. The total weight of the transmitter will be approximately 2 lb. Figures 21 and 22 show the two sides of the first module. Figure 23 shows the power-amplifier side of the second module (foreground) contrasted with a module from a typical *Ranger-Mariner*-class transponder. Both of the ruggedized modules have survived 10,000-*g* peak-amplitude impacts from 180 ft/sec in all principal directions. The third module (two doublers) is still under electrical development. However, few problems should be experienced under impact, since the unit will utilize strip-line techniques.

Perhaps the most difficult problem in ruggedizing transmitters has been the development of impact-resistant

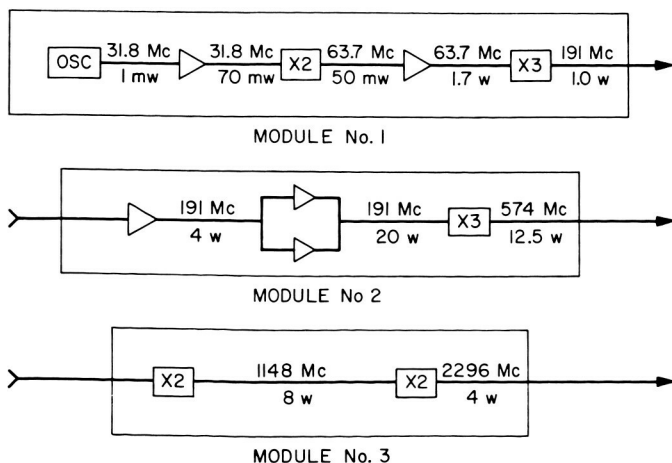


Fig. 20. S-band transmitter schematic

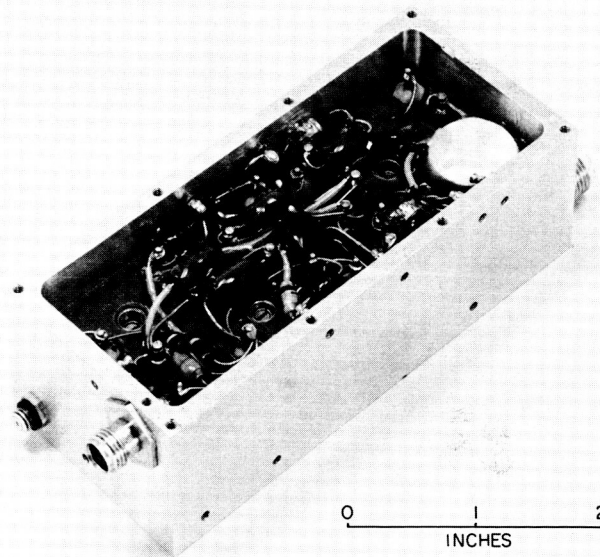


Fig. 21. DC side of Module No. 1—S-band transmitter

crystals. Figure 24 shows a high-impact crystal being developed through a contract with the Valpey-Fisher Co. This crystal is contained in the first module of the S-band transmitter. The original specifications called for a nominal frequency of 19.125 Mc $\pm 0.001\%$ at 25°C. The crystal was to utilize design techniques applicable over the frequency range from 15 to 50 Mc, have an impedance value less than 30 ohms at 25°C, a capacitance between leads of less than 7 $\mu\mu\text{f}$, and a temperature frequency deviation of no more than 0.001% over the temperature range from -10°C to 75°C . Since the crystal is designed for use in a phase-coherent system, requirements on phase error were also extremely tight. Prototype

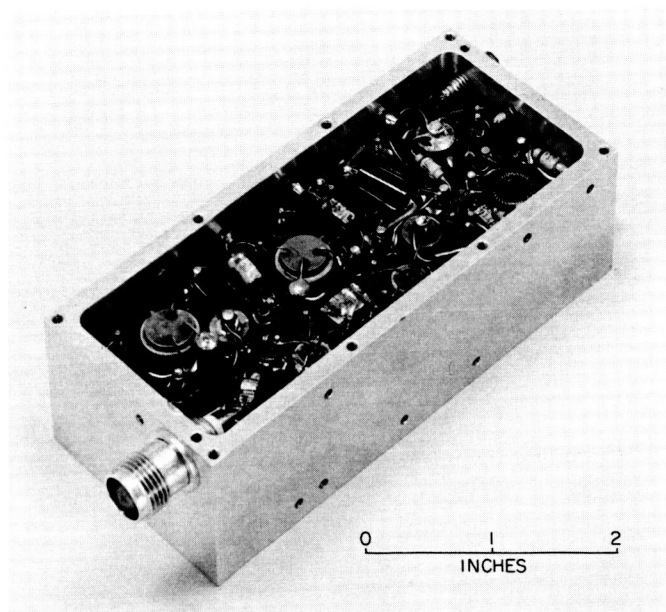


Fig. 22. RF side of Module No. 1—S-band transmitter

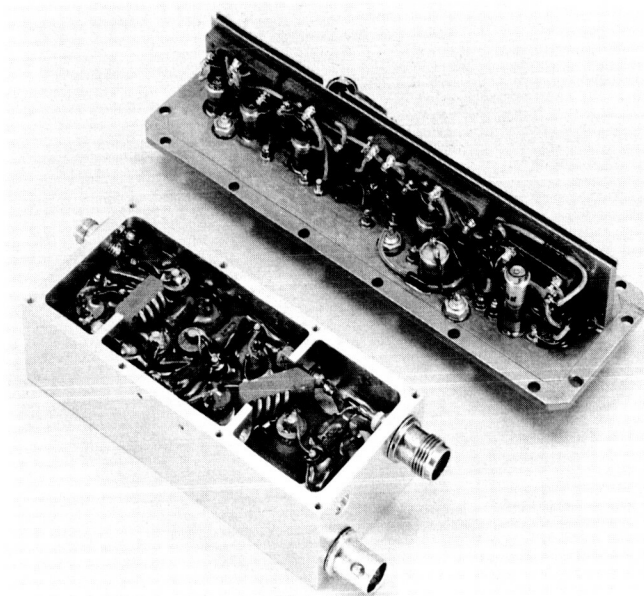


Fig. 23. Module No. 2 (foreground)—S-band transmitter

models of the crystal have been delivered not only at the 19.125-Mc frequency, but also at a 21.3-Mc frequency.

The crystal holder allows the quartz element to resonate sufficiently to fulfill its function, yet constrains it so that it will not deform to failure under impact. Prototype crystals have been tested in all principal directions at impacts of up to 12,000 *g*'s peak amplitude from 200

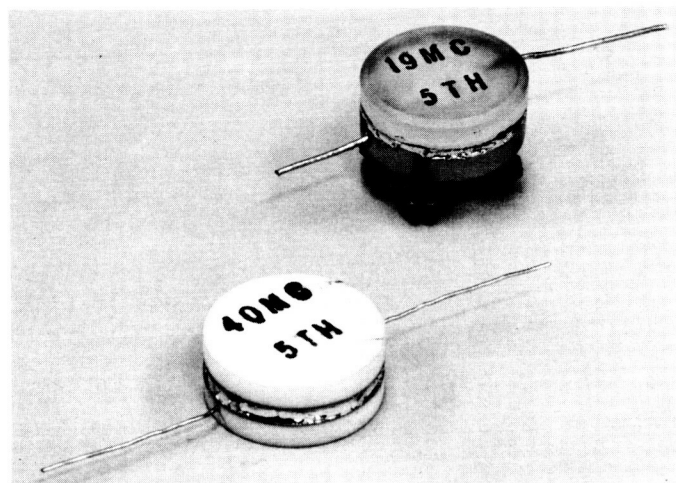


Fig. 24. High-impact crystal

ft/sec. Failures were encountered in early models with the seal and with the mounting techniques. However, later prototypes have survived 10,000-*g* impacts with only a few hundred cps change in frequency. The crystal-body halves are made of alumina. The sealing surfaces are coated with vacuum-deposited chrome-silver. Leads are brazed into moly-manganese-coated holes in the crystal body halves. Contact surfaces of gold over silver are then vacuum-deposited over the lead ends on the body halves. Contact surfaces on the quartz element are

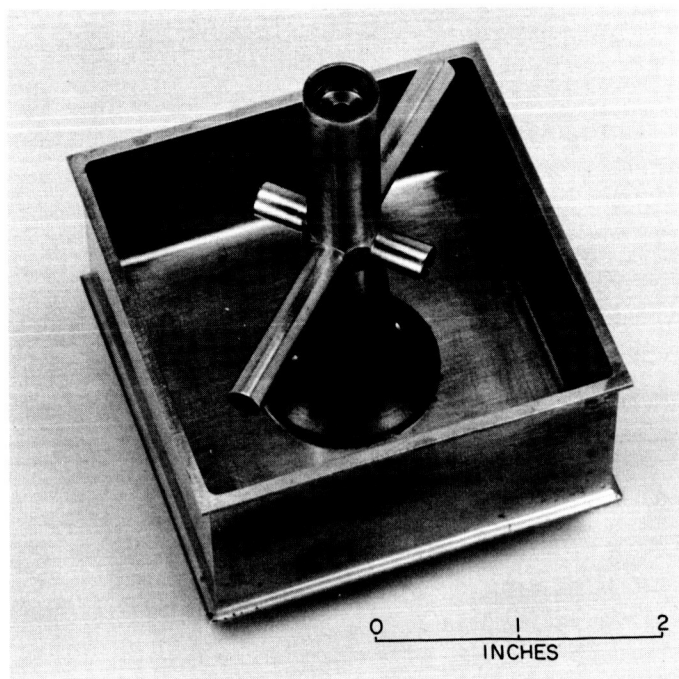


Fig. 25. Ruggedized S-band turnstile antenna

also gold deposited over silver. The crystal is assembled by clamping the quartz element between the body halves and then soldering the body together with eutectic solder.

Figure 25 is a ruggedized turnstile S-band antenna which has survived impacts of 9,000 *g*'s peak amplitude from 170 ft/sec with no significant mechanical or elec-

trical damage. The antenna weighs 3½ oz. A Sanders Associates Model AS-63 spiral antenna has successfully survived impacts up to 5,000 *g*'s from 100 ft/sec in all principal directions. This antenna was not designed for impact use. Failure at 7,000 *g*'s occurred because of deflections in the spiral element. A ruggedized version of this antenna has successfully withstood impacts of 10,000 *g*'s peak amplitude.

VI. BATTERIES

This is a joint effort between the Engineering Mechanics Division and the Guidance and Control Division. The intent of this effort is to develop and qualify high-performance (silver-zinc and silver-cad) sealed batteries which can withstand the 10,000-*g* environment. To date, the program has been concerned mainly with evaluating either off-the-shelf batteries or batteries developed for other spacecraft uses. Table 1 summarizes the testing to date. In all cases, individual cells were potted into rigid (typically ⅜-in.-thick aluminum) fixtures and impacted in all principal directions. Figure 26 indicates the impact directions.

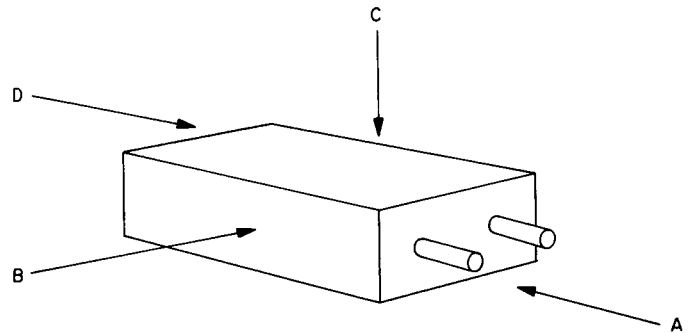


Fig. 26. Battery impact acceleration directions

Table 1. High-impact battery tests

Battery	Condition	Potting	Direction	<i>g</i> level	ΔV , ft/sec	Comments
Yardney LR20-3X-1	25% cap.	Silastic	A	1,800 pk	50	No detectable degradation
	25% cap.	Silastic	B	1,800 pk	50	
	25% cap.	Silastic	C	1,800 pk	50	
	25% cap.	Silastic	A	4,100 pk	135	
Yardney LR20-3X-1	25% cap.	Silastic	A	1,480 pk	52	No detectable degradation
	25% cap.	Silastic	D	3,500 pk	120	Would not charge to capacity
Yardney LR20-3X-1	25% cap.	Silastic	C	3,400 pk	117	Capacity slightly degraded
Recased Yardney	25% cap.	Silastic	C	4,200 pk	108	No detectable degradation
	25% cap.	Silastic	A	7,300 avg	175	Battery destroyed—zinc plates failed, silver plates cracked
	25% cap.	Silastic	B	7,300 avg	175	
	25% cap.	Silastic	C	7,300 avg	175	
Eagle Picher Model 25-65 silver-zinc	Uncharged	Silastic	C	4,800 pk	145	Slight visible plate damage; no shorting
	Uncharged	Silastic	D	4,800 pk	145	Plates buckled
Eagle Picher Model 25-65	Charged	Silastic	C	3,900 pk	130	No detectable degradation
	Charged	Silastic	C	4,600 pk	152	
	Charged	Silastic	C	5,750 avg	148	
	Charged	Silastic	C	8,220 avg	149	
	Charged	Silastic	B	3,700 pk	135	
	Charged	Silastic	B	5,700 avg	150	Case split, one plate buckled; discharge cycle showed almost full capacity

Table 1. High-impact battery tests (Cont'd)

Battery	Condition	Potting	Direction	g level	ΔV , ft/sec	Comments
Eagle Picher Model 25-65	Charged	Epon 815	B	7,000 pk	148	No detectable degradation
	Charged	Epon 815	B	8,800 pk	143	Case cracked and separated from potting; plates crushed, internal short-circuit
Yardney YS 20 silver-cad cell	Charged	Silastic	B	5,700 pk	167	No detectable degradation
	Charged	Silastic	C	7,400 pk	166	No detectable degradation
	Charged	Silastic	B	7,200 pk	167	No detectable degradation
	Charged	Silastic	B	10,800 pk	169	Case cracked; no electrical degradation
Yardney YS 20 silver-cad cell	Charged	Silastic	B	7,600 pk	174	Case cracked; no electrical degradation
Whittaker P.S.D. PN 201171 sealed silver-cad cells 2 potted in fixture	Charged	Epon 815	B	8,400 pk	161	Case cracked; no electrical degradation
MA-C ESB cell	Charged		D	5,400 avg	158	Case cracked; gross internal shorting
Whittaker P.S.D. CD-3 sealed silver-cad cells 2 potted in fixture	Charged	Epon 815	B	10,800 pk	174	No detectable degradation
	Charged	Epon 815	D	10,400 pk	170	No detectable degradation
	Charged	Epon 815	C	10,000 pk	166	No detectable degradation
	Charged	Epon 815	A	10,800 pk	176	No electrical degradation
Whittaker P.S.D. CD-3 sealed silver-cad cells 2 potted in fixture	Charged	Epon 815	A	10,000	164	Potting and one case cracked
	Charged	Epon 815	A	10,000	164	No electrical degradation
Ranger ESB cell	Charged	Epon 815	D	6,000 pk	165	Potting and one case cracked
Whittaker P.S.D. CD-3 sealed silver-cad cells 2 potted in fixture	Charged	Epon 815	A	6,800 pk	170	Case cracked; internal shorting
	Charged	Epon 815	A	9,800 pk	176	Potting and case cracked, plates shifted
Plates in bag potted in structure	Charged	Epon 815	Edgewise	11,600 pk	135	Potting and case cracked
ESB 6-cell	Charged	Epon 815	C	5,000 pk	107	No internal damage
ESB 6-cell	Charged	Epon 815	D	5,000 pk	107	Battery was destroyed
ESB 6-cell	Charged	Epon 815	B	5,000 pk	108	Survived
ESB 6-cell	Charged	Epon 815	C	8,000 pk	115	Survived
ESB 6-cell	Charged	Epon 815	D	7,200 pk	117	Survived
Yardney HR-1 2 cells potted in fixture	Charged	Solithane 8	A	8,000 pk	122	Failed
	Charged	Solithane 8	A	6,300 avg	122	
	Charged	Solithane 8	C	6,920 avg	148	
	Charged	Solithane 8	B	6,910 avg	148	
	Charged	Solithane 8	B	9,000 pk	166	Case cracked
	Charged	Solithane 8	C	9,000 pk	179	No electrical degradation
	Charged	Solithane 8	D	10,800 pk	167	
	Charged	Solithane 8	A	12,000 pk	171	
Gould Ni-cad button cells in 6-v (100 B) and 12-v (500 BH) stacks	Charged	828/D	Axially and laterally	6,000 pk	110	No detectable degradation
	Charged	828/D		8,500 pk	170	Intermittants occurred when impacted axially with acceleration in the positive (+) direction

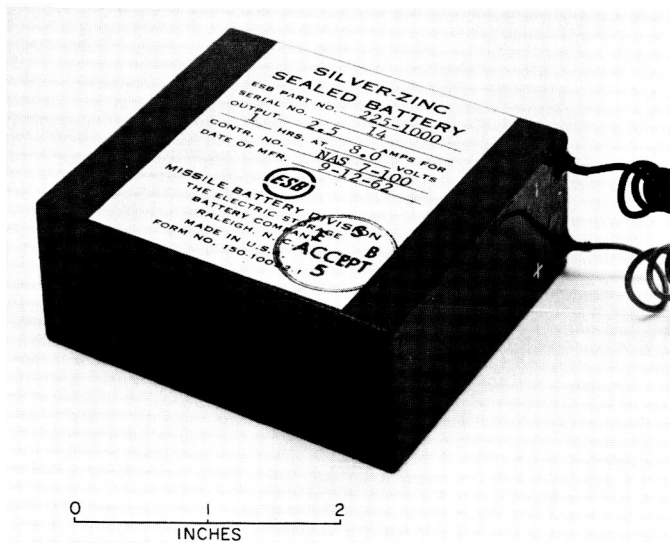


Fig. 27. Six-cell battery before impact

Initially, the investigation centered around plates and separators, since these are essential to batteries and less susceptible to various structural approaches than cases. Discharged silver-zinc batteries are much less rugged than charged batteries because the anode is in the oxidized condition. Early tests performed with discharged batteries resulted in gross plate failures which seemed to

indicate that additional structure was required in the plates themselves. However, later tests have shown that charged plates are sufficiently strong to survive impact if properly supported. In no case have the separator materials been damaged under impact. Since batteries used in landed payloads would undoubtedly be charged at impact, the feeling at this time is that 10,000-g-resistant batteries can be manufactured with conventional plate and separator techniques, providing that cases and internal potting can provide adequate and rigid support. The high-impact battery program is, therefore, presently involved in developing improved case designs and potting techniques.

Figure 27 shows a small, 6-cell, sealed, silver-zinc battery which was tested under impact. After surviving 5,000 g's peak amplitude in all principal directions, it failed when impacted at 8,000 g's peak amplitude with the plate lead trailing. Figure 28 shows two of the plates after impact. The damage is typical. The reason for failure was breakage of the plate leads due to crumbling of the plates and subsequent grid failure. The battery would have been electrically within specification had these leads not failed. This battery was not designed to take high impacts, and could have been easily ruggedized either by providing more slack in the internal leads, designing the case to hold the plate stacks more firmly, or potting internally.

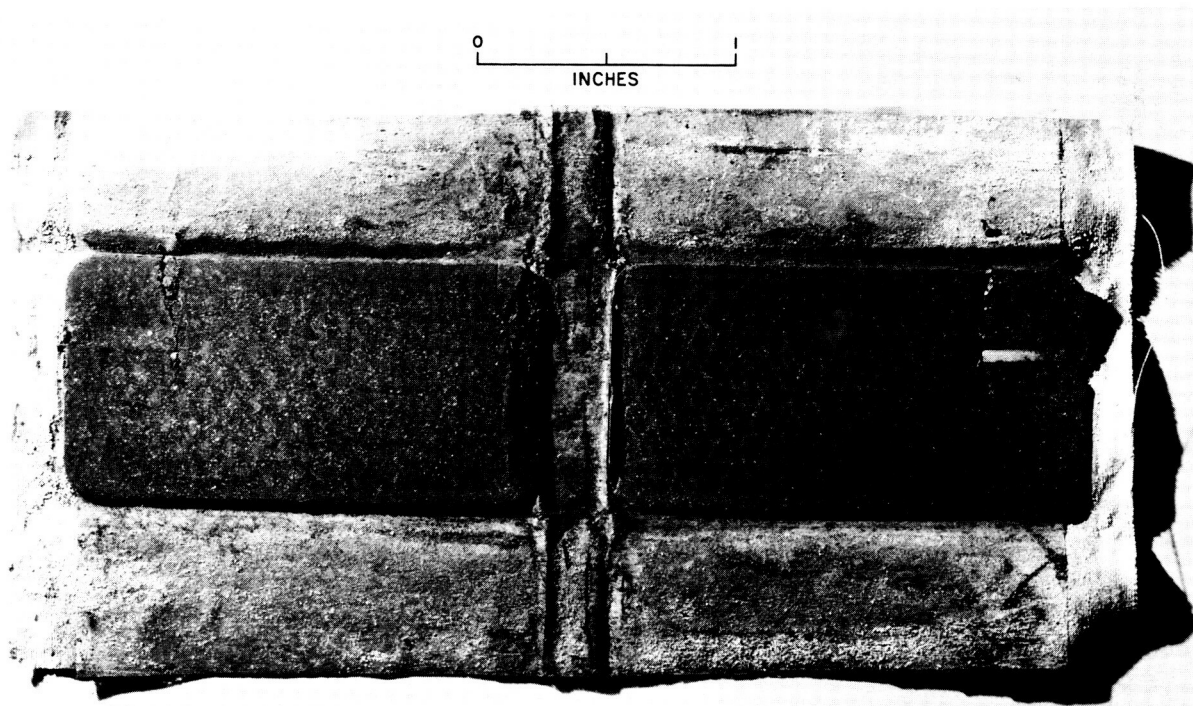


Fig. 28. Six-cell battery plates after impact

VII. MECHANISMS

Several high-impact-resistant mechanisms have been developed and tested by the Engineering Mechanics Division during this Report period. The pressure regulator and sample valve for the gas chromatograph have been discussed in Section IV of the Report. Figure 29 shows an alternate sample valve which was built and successfully tested to 5,000 g's. This valve is powered by a "spirator" spring which stores sufficient energy for 45 cycles (15 complete gas chromatograph analyses). The unit weighs 8 oz and can be triggered by a small solenoid.

The design of the above mechanisms required that all parts be sturdy enough to survive the impact and that all bearing points be adequately sized. In some mechanism problems, it is quite difficult to provide adequate bearing

area to prevent damage. A good example is the bearing problem encountered in an electric motor for space application. The rotor must be massive and closely positioned and rolling element bearings are advantageous. Preliminary work with bearings and bushings for such use indicated that it was impractical to expect conventional bearing practices to support objects such as motor rotors at g levels on the order of 10,000. Table 2 shows typical data from early tests. In these tests the bearings were mounted in pairs in an aluminum block and weighted with shafts of 1.25 oz each. The shock loads were applied in radial and axial directions. The shafts were not turning during impact. The ball bearings were 0.25 in. ID, 0.625 in. OD, phenolic separator, flanged deep-groove Barden bearings. The bushings were machined from a Westinghouse sintered copper-lead-teflon compound.

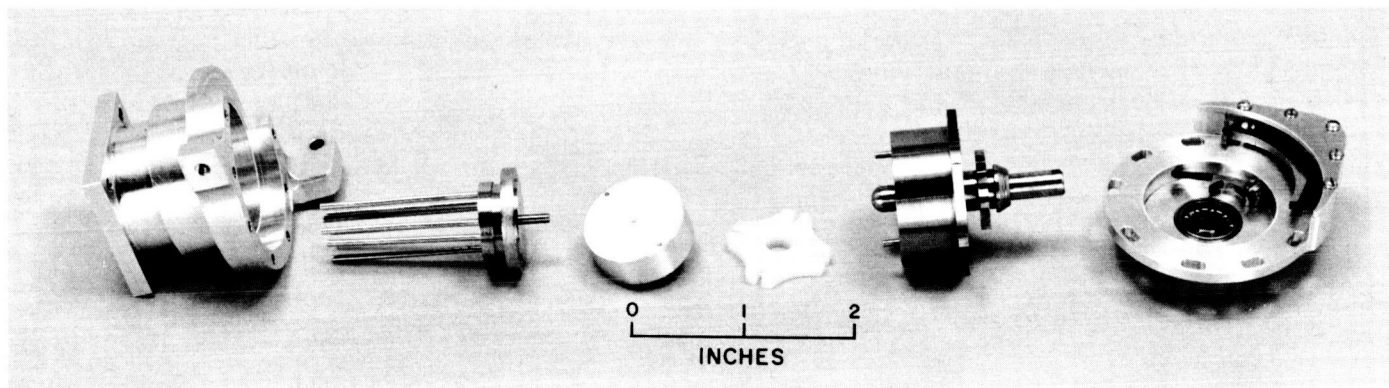


Fig. 29. Alternate gas-chromatograph sample valve

Table 2. Impact tests of ball bearings and bushings

Impact			Ball bearings			Bushings		
Velocity, ft/sec	Peak accel- eration, g's	Direction	Radial play, in.	End play, in.	Torque, in.-oz	Radial play, in.	End play, in.	Torque, in.-oz
50	300	Radial	Negligible	0.000	0.50	Negligible	0.001	0.75
		Axial	Negligible	0.000	0.50	Negligible	0.001	0.75
50	700	Radial	Negligible	0.000	0.50	Negligible	0.001	0.85
		Axial	Negligible	0.000	0.50	Negligible	0.006	0.75
50	1500	Radial	Negligible	0.000	0.50	0.001	0.0075	0.85
		Axial	Negligible	0.000	0.50	0.001	0.008	0.85
50	3000	Radial	Negligible	Very rough	0.75	0.0015	0.008	0.75
		Axial	Negligible	Very rough	0.75	Bushing locked		
50	6000	Radial	Bearing brinelled so severely races locked					
		Axial						

Since rolling element bearings are very attractive for use in space, an investigation was made of methods of supporting bearings so that impact loads are not transmitted through the rolling elements. Figure 30 shows a prototype bearing mount for a rotating element bearing. This mount is a six-degree-of-freedom spring which is stiff enough (approximately 25,000 lb/in. axially and radially) to maintain alignment yet soft enough to deflect during an impact so that bearing loads will not become high enough to damage the bearing. A 4-oz rotating mass with a 0.002-in. clearance with its housing was supported between two lightweight ball bearings (Microtech MC814SSR 25L10) in these spring mounts. The unit survived impacts of 10,000 g's peak amplitude from 200 ft/sec with no detectable bearing damage. The major loads, of course, were absorbed by bottoming between the rotating mass and the housing.

A series of small electric motors incorporating spring-mounted bearings was developed and tested. Figure 31 is an exploded view of one of these motors. This is a rebuilt Gaylord-Rives Size 8 synchronous motor and has successfully survived 10,000-g impacts from 200 ft/sec in both radial and axial directions. The motor was not operating during impact. It was rigidly clamped to the carriage of the testing machine. Acoustic techniques were used to compare preshock and postshock performance as well as torque measurements. Pickups were attached to the motor which was operated in a sound-proof chamber.

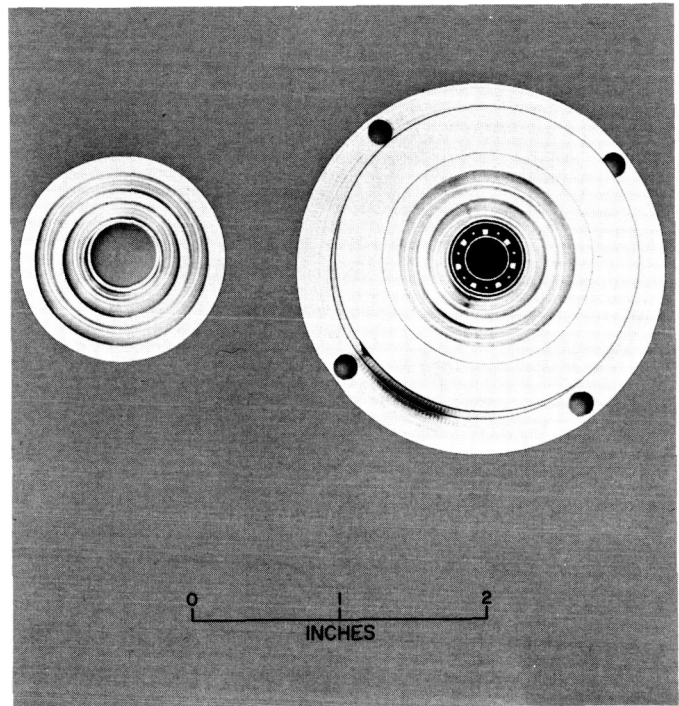


Fig. 30. Bearing spring mount

The resulting noise spectrum was then analyzed. By looking at the energy content of various frequencies it was possible to detect extremely small changes in bearing performance.

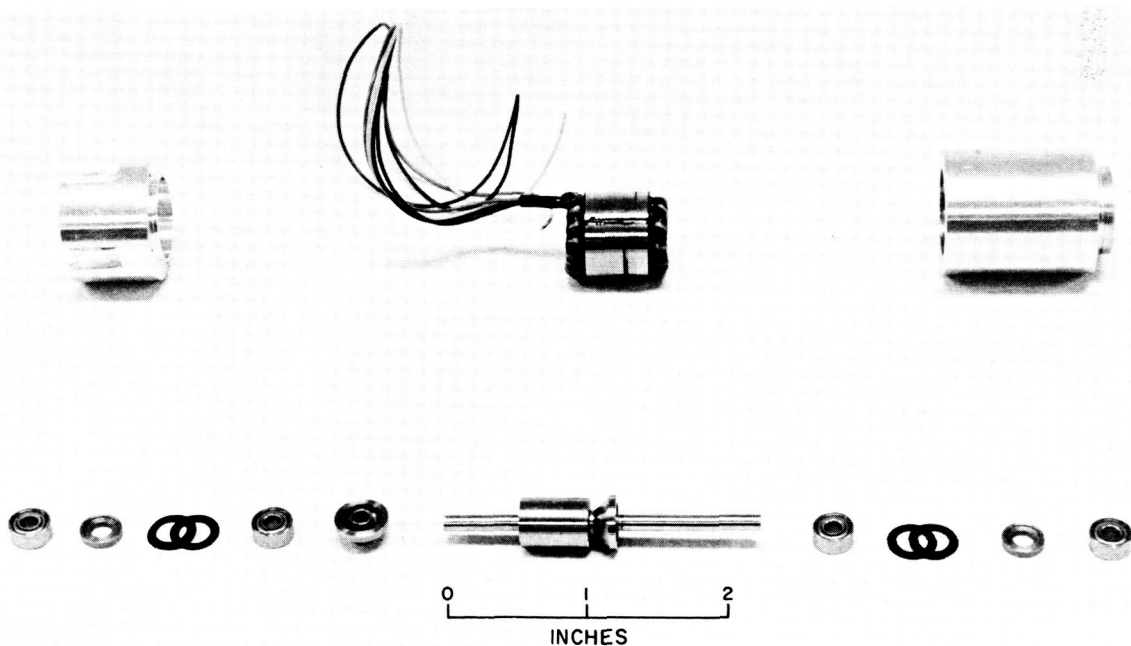


Fig. 31. Exploded view of ruggedized motor

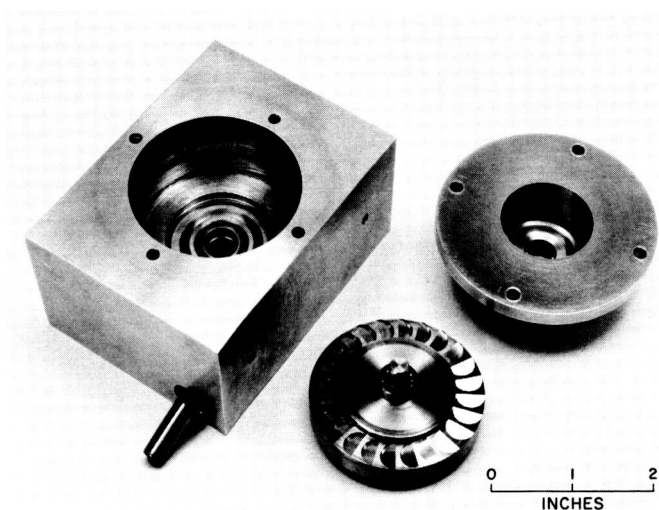


Fig. 32. High-impact-resistant turbine

One possible use of bearings in a high-impact situation would be in a hard-landed turboalternator secondary power source. In this situation it is conceivable that the turboalternator would be operating during impact. In an attempt to investigate this situation, a mocked-up turbine was fabricated and tested (Fig. 32). The turbine was similar to the test specimen for the bearing spring mounts referred to above. Turbine buckets were milled into the rotating mass and an air jet was provided to power the turbine. By providing air through flexible tubing, it was possible to power the turbine continuously before, during, and after impact. The unit was impacted axially and radially at 10,000 g 's from 165 ft/sec. Although the rotating speed changed slightly during impact, the device regained its preimpact rotating speed (about 30,000 rpm) and operated successfully for a 3-5-hr period before it was shut down. Examination showed that no significant bearing damage had taken place. Damage to the turbine and housing was small.

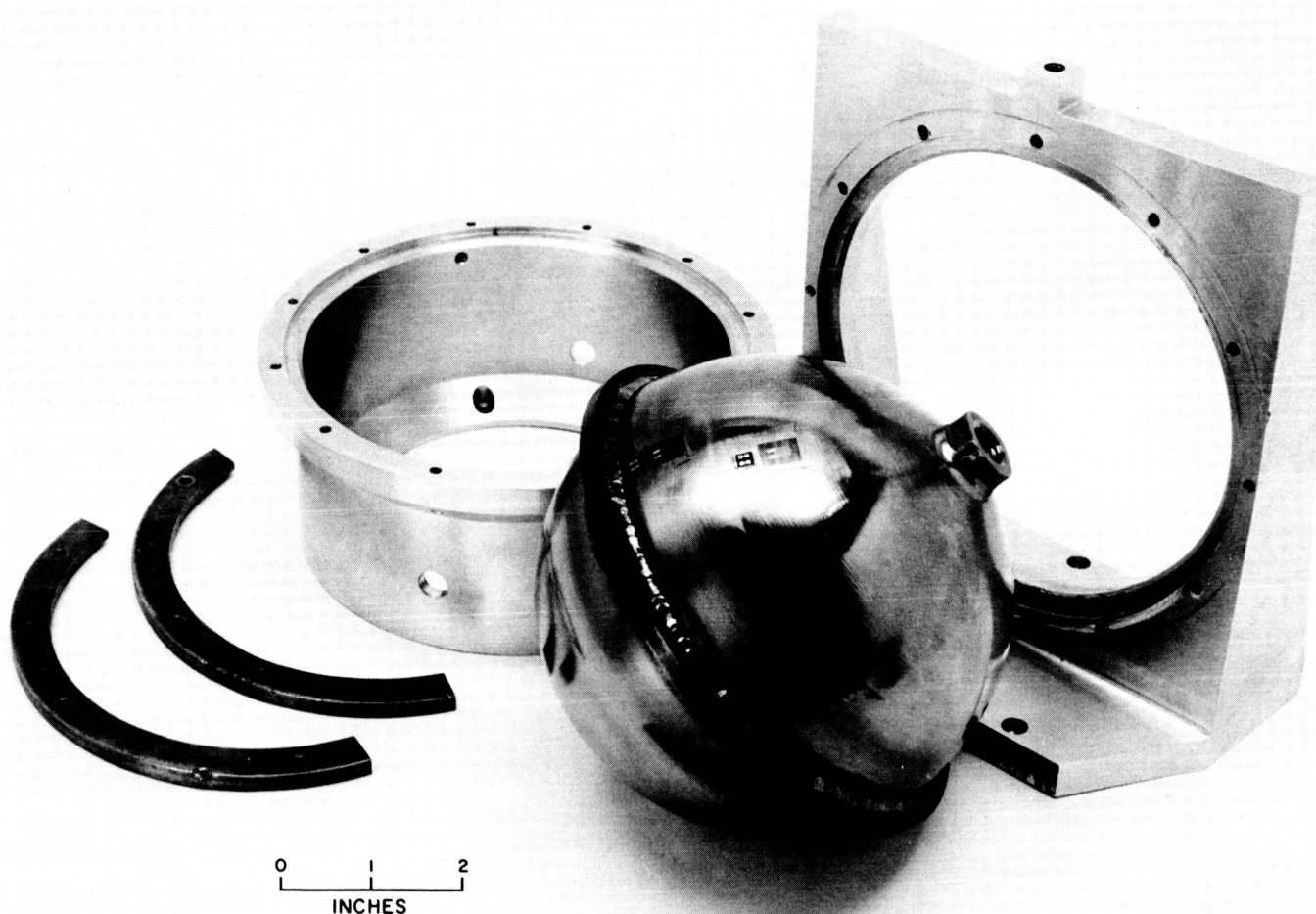


Fig. 33. Pressure vessel and fixtures after test

As a complementary effort, a titanium pressure vessel was tested under high impact. Figure 33 shows the tank and the fixtures in which it was mounted. A 0.200-in.-thick \times 0.300-in.-wide titanium ring was welded to the circumference of the tank. The tank was then clamped in the fixture by this ring and impacted both normal to

the ring and parallel to the ring. It was tested empty at impact levels up to and including 10,000 g's from 150 ft/sec with no apparent damage. It was then pressurized to 3,000 psi with water and impacted in both directions at 10,000 g's from 140 ft/sec. There appeared to be no damage to the tank.

VIII. MISCELLANEOUS ELECTRONIC COMPONENT TESTING

This section summarizes the electronic-component testing which has been performed during this Report period. This testing was for the purpose of investigating various components whose impact survival capabilities were unknown. The majority of the components were needed for the gas-chromatograph development. As in the component testing covered in Ref. 1, samples were small and functional tests performed before and after impact did not always constitute a complete evaluation. These tests should, therefore, be considered as feasibility investigations, rather than component-parts qualifications.

A. Capacitors

A sample of four Goodall 617-G-1 1- μ f 50-v mylar capacitors was tested at various levels up to and including a peak amplitude of 10,000 g's from 200 ft/sec. The capacitors were clamped in a rigid fixture for testing. No degradations in electrical characteristics were detected as a result of the impacts.

A sample of 20 Sprague 150-D solid-slug B-size tantalum capacitors (ten 4.7- μ f/50-v and ten 15- μ f/20-v) was tested at various levels up to and including a 10,000-g average amplitude from 190 ft/sec. The capacitors were mounted between terminals on a terminal board and secured to the board with a coating of Solithane. The specimens were oriented so that half were impacted longitudinally and half transversely. Measurements of forward voltage drop and reverse voltage breakdown before and after impact showed no appreciable change.

B. Diodes

A sample of three Microwave Associates PV 006 diodes and three Microwave PV 009 diodes was impacted. The diodes were stud-mounted and impacted both axially

and transversely at levels up to and including 10,000 g's peak amplitude from 180 ft/sec. No mechanical damage or electrical degradation was observed.

C. Microcircuits

A sample of one specimen each of several microcircuits was impact-tested. The microcircuits were a Signetics SE-101 gate, a Signetics SE-124 flip-flop, a Texas Instruments SN 530 flip-flop, a Motorola MC 301F gate, a Westinghouse WS 217 gate, and a Westinghouse WS 235 flip-flop. The microcircuits were all in flat-packs and were cemented to the test fixture with Duco cement. Impacts at 7,000 g's peak amplitude from 120 ft/sec both normal to the plane of the devices and parallel to the device leads caused no observable mechanical damage. The devices were then impacted at 12,500 g's peak amplitude from 200 ft/sec both normal to the plane of the devices and parallel to the device leads. After these impacts, the two Signetics devices, the Texas Instrument device, and the Motorola device were found to be electrically unimpaired. The case of the SE-101 gate had chipped. No mechanical damage could be found on the SE-124 flip-flop, the SN-530 flip-flop, or the MC 301F gate. The two Westinghouse devices were destroyed. The tops came off of the cases, the cases broke, and the chips were loosened. Figure 34 shows one of these devices after impact.

D. Resistors

A sample of 18 Texas Instruments CG 1% resistors in $\frac{1}{8}$ -w, $\frac{1}{4}$ -w, and $\frac{1}{2}$ -w sizes was impact-tested. The resistors were mounted between terminals and secured to the terminal board with a coating of Solithane. They were impacted both axially and transversely at levels up to

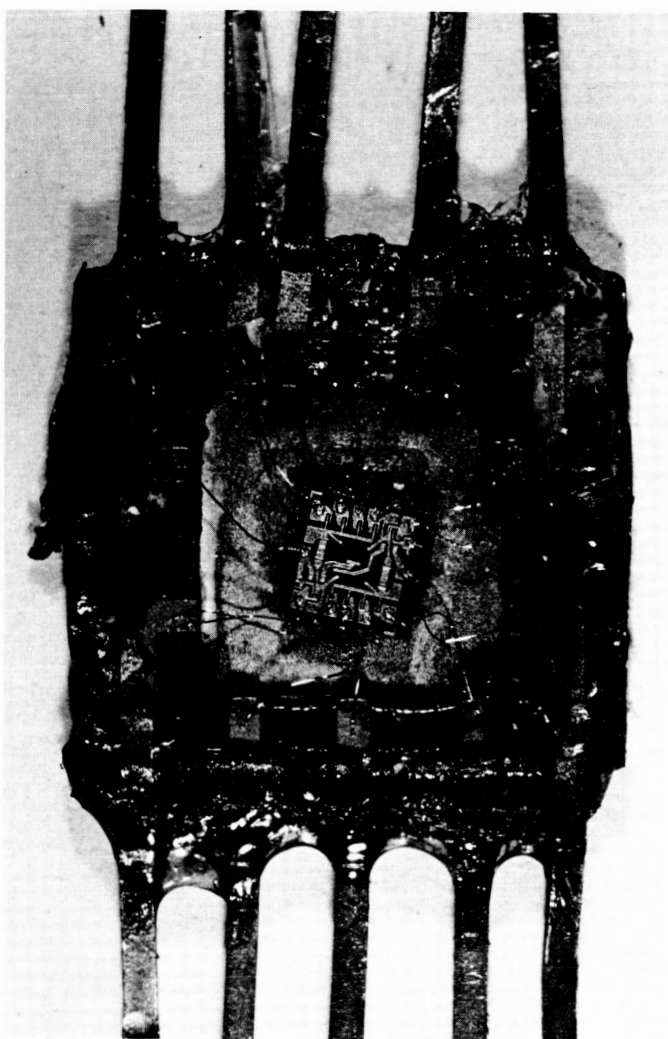


Fig. 34. Integrated circuit after test

and including a peak amplitude of 10,000 g 's from 200 ft/sec. These tests produced no observable failures.

A sample of 8 Victoreen Hi-Meg glass-cased resistors was tested at a peak impact level of 10,000 g 's from 200 ft/sec. Resistors were mounted so that specimens were impacted both axially and transversely. The resistors mounted transversely to the impact direction failed due to fracture of the resistive element. Victoreen provided two alternate solutions to a more rugged resistor. One was a miniaturized version and the other supported the resistive element with a Teflon sleeve. A sample of five of the miniaturized version and four of the sleeved version survived axial and lateral impacts up to and including an estimated peak amplitude of 10,000 g 's from 200 ft/sec with no detectable damage. Figure 35 shows these resistors mounted on the test block after the tests.

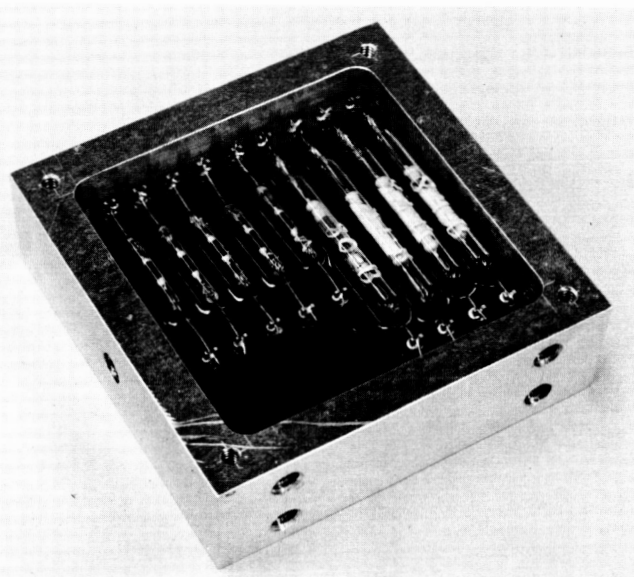


Fig. 35. Hi-Meg resistors after test

E. Transistors

Four each of Texas Instrument 2N930, 2N2605, 2N3350, 2N2432, and 2N3329, Fairchild 2N3117, and Solid State Products 2N2843 transistors were mounted in close-fitting holes in a block of aluminum. The transistors were oriented so that during impact one of each type would be impacted with the leads trailing, one with the leads leading and two transversely in normal directions. The block was first impacted at 4,400 g 's from 105 ft/sec with no failures. An impact at 6,300 g 's from 110 ft/sec caused one of the TI 2N3329 transistors which was mounted laterally to the direction of impact to fail. An impact at 7,400 g 's from 185 ft/sec caused one of the TI 2N930 and one of the TI 2N3350 transistors which were mounted laterally to the impact to fail. An impact at 9,100 g 's from 175 ft/sec caused one Fairchild 2N3117 transistor mounted laterally to the impact to fail. A final impact at 10,000 g 's from 175 ft/sec caused no failures. All failures occurred at the bond between the lead wires and the semiconductor chip. Figure 36 shows a typical failure. All failed transistors were replaced with one of the same type before the next test was conducted. For the last two tests the block was rotated from its orientation for the first three tests, in order to test the various individual transistors in various planes. During the last three tests, three TI 2N3609 transistors were included. No failures of this particular device occurred.

A series of transistors was screened for use in the prototype gas chromatograph by being impacted laterally (normal to the leads) at 10,000 g 's from an impact speed of 180 ft/sec. A total of 28 Amelco 2N2979's, 17

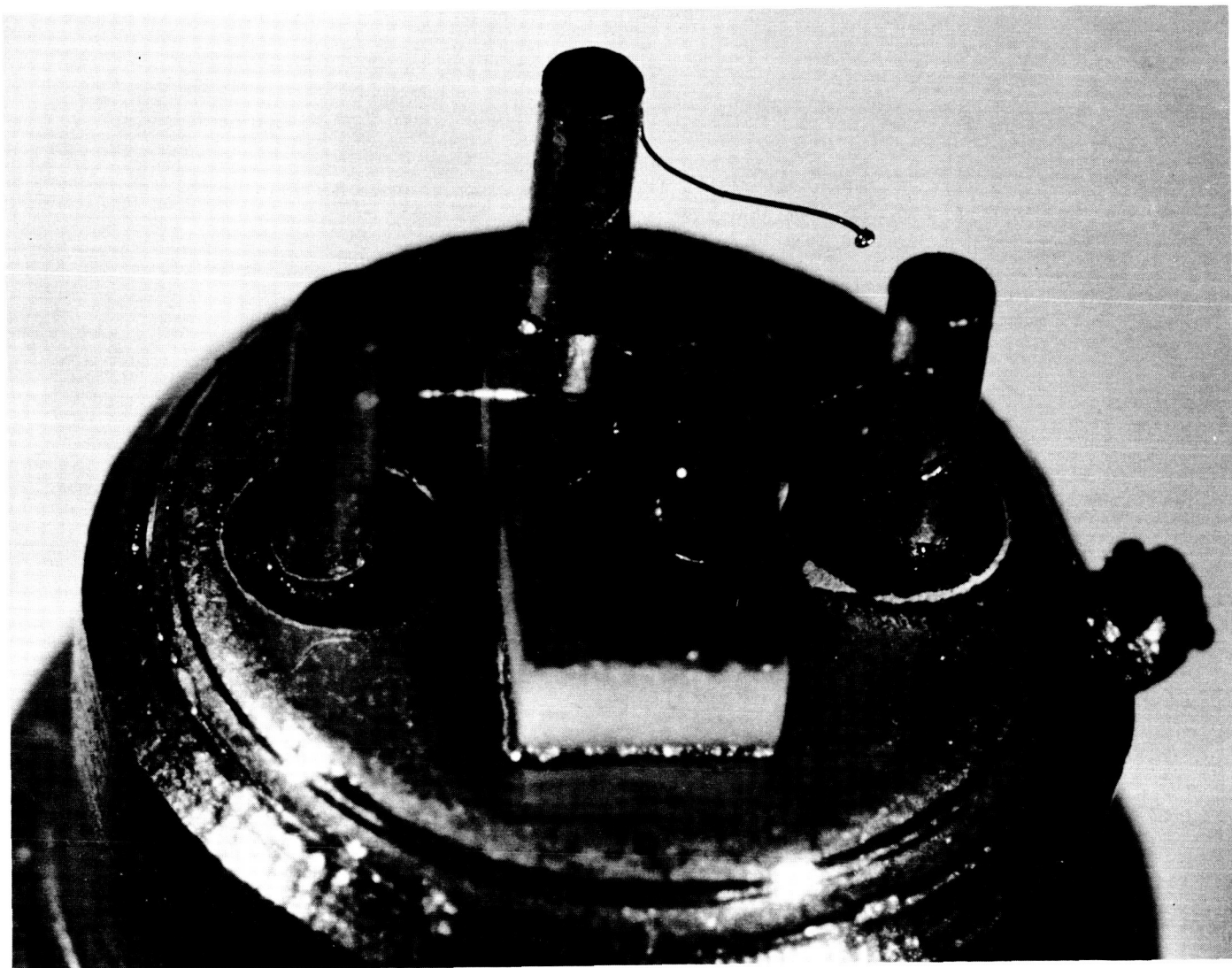


Fig. 36. Transistor failure

TI 2N2605's, eight TI 2N3350's, ten TI 2N930's, 21 Fairchild 2N930's and six SSP 2N2843's were tested. One FA 2N930 and one Amelco 2N2979 failed. Both failures were at the bond between the transistor chip and the lead wire.

A sample of three RCA 2N3375, three RCA 2N3553, and three RCA 2N3632 transistors were impacted longitudinally and transversely at levels up to and including 10,000 *g*'s peak amplitude from 180 ft/sec. No mechanical damage or electrical degradation was observed.

REFERENCES

1. Jacobsen, L. S., and Ayre, F. S., *Engineering Vibrations*, New York: McGraw-Hill Book Co., Inc., 1958.
2. Fung, Y. C., and Barton, M. V., "Some Shock Spectra Characteristics and Uses," *Journal of Applied Mechanics*, September 1958, pp. 367-372.
3. Brooks, R. O., *Shock Testing Methods*, Sandia Corporation Technical Memorandum SCTM 172A-62(73), Albuquerque, N.M., September 1963.
4. Lonborg, J. O., *High Impact Survival*, Jet Propulsion Laboratory Technical Report No. 32-647, Pasadena, Calif., September 30, 1964.